Lunar Elemental Analysis Obtained From the Apollo Gamma-Ray and X-Ray Remote Sensing Experiment

J. I. Trombka
Goddard Space Flight Center
Greenbelt, Maryland

J. R. Arnold
University of California, San Diego
La Jolla, California

I. Adler
University of Maryland
College Park, Maryland

A. E. Metzger
Jet Propulsion Laboratory
Pasadena, California

R. C. Reedy
Los Alamos Scientific Laboratory
Los Alamos, New Mexico

Gamma-ray and X-ray spectrometers carried in the Service Modules of the Apollo 15 and Apollo 16 spacecraft were employed for compositional mapping of the lunar surface. The measurements involved the observation of the intensity and characteristic energy distribution of gamma rays and X-rays emitted from the lunar surface. A large-scale compositional map of over 10 percent of the lunar surface was obtained from an analysis of the observed spectra. The Apollo 15 flight was at a lunar orbital inclination of 29 degrees as compared with a 9-degree inclination of the Apollo 16 flight; thus, the projected ground track of the Apollo 15 flight covered a larger projected surface area than that of the Apollo 16 flight.

The objective of the X-ray experiment was to measure the K spectral lines from Mg, Al, and Si. Spectra were obtained and the data were reduced to Al/Si and Mg/Si intensity ratios and ultimately to chemical ratios. Analyses of the results have indicated (1) that the Al/Si ratios are highest in the lunar highlands and considerably lower in the maria, and (2) that the Mg/Si concentrations generally show the opposite relationship. There is a tendency for the Al/Si values to increase from the western mare areas to the eastern limb highlands. There are distinct chemical contrasts between such features as the small mare basins and the highland rims.

The objective of the gamma-ray experiment was to measure the natural and cosmic-ray-induced activity emission spectrum. At this time, the elemental abundances for Th, U, K, Fe, Ti, Si, and O have been determined over a number of major lunar regions. Regions of relatively high natural radioactivity were found in the Mare Imbrium and Oceanus Procellarum regions. High spots of natural radioactivity were also found south of Fra Mauro, somewhat southwest of Archimedes, and south of Aristarchus. An enhanced region of natural radioactivity was found around Van de Graaff on the far side of the Moon. In regions other than Mare Imbrium and Oceanus Procellarum, an anticorrelation between natural radioactivity and lunar elevation, as determined from the Apollo laser altimeter, has been found.

From the combined results of the gamma-ray and X-ray spectrometer experiments almost complete information concerning the major element composition of over 10 percent of the lunar surface has been obtained. Distributions have also been mapped for K, Th, and Ti. Interesting correlations between lunar topography and magnetic and gravitational properties have been found.

Gamma-ray and X-ray fluorescent spectrometers carried in the Service Modules of the Apollo 15 and Apollo 16 spacecraft were employed for compositional mapping of the lunar surface. The measurements involved the observation of the intensity and characteristic energy distribution of gamma rays and X-rays emitted from the lunar surface. The objective of the X-ray experiment was to measure the K spectral lines from Mg, Al, and Si, while that of the gamma-ray experiment was to measure the natural and cosmic-ray-induced emission spectrum. At this time it is possible to obtain large-scale compositional maps of over 10 percent of the lunar surface for Al, Mg, Th and U, K, Fe, Ti, Si, and O. The Apollo 15 flight was at a lunar orbital inclination of about 29 degrees as compared with about a 9-degree inclination of the Apollo 16 flight; thus, the projected ground track of the Apollo 15 flight covered a larger surface area than that of the Apollo 16 flight.

Over the past two years, certain results of these Apollo gamma-ray and X-ray remote sensing experiments have appeared in the literature. This report will present a summary of the results and indicate the present methods employed in the analysis of the data. It is hoped that this summary of both the analytic methods and results will enable other investigators in planetology to make optimum use of the results.

Instrumentation and Data Analysis, Gamma-Ray Experiment

The gamma-ray spectrometer consisted of a 7- by 7-cm right cylindrical NaI (Tl) crystal detector with a plastic anticoincidence mantle to suppress response to charged particles, and a 512-channel, pulse-height analyzer including an amplifier, but no memory. The information was transmitted event by event in real time or, if necessary, was stored on a magnetic tape for later transmission to Earth. Spectra were obtained by accumulating the pulses received on Earth for various periods of time. Details of the experimental system are described in Arnold et al. (ref. 1) and Harrington et al. (ref. 2). The instrument was mounted on a boom capable of extending 7.6 m from the spacecraft in order to minimize background interference due to gamma-ray emission from the spacecraft.

The model on which the data analysis is based can be found in a research paper by Reedy, Arnold, and Trombka (ref. 3). The experimental data as received from the Johnson Space Center were processed for analysis by eliminating those data having parity errors and other problems and analytically shifting to a constant level of gain. (The overall instrument gain decreased over 40 percent on Apollo 15 and about 10 percent on Apollo 16 during the lunar phase of the mission.) The gain as adjusted for analysis was about 19 keV/channel. The spectra were then corrected for solid angle to a constant height of 110 km above the lunar surface. All data obtained over each region to be analyzed were then accumulated into master spectra. An initial background correction was made for the general sky background of gamma radiation, for natural gamma-ray emission, and for cosmic-ray-induced gamma-ray emission from the spacecraft, local mass around the detector, and the detector itself. The background level was determined from measurements made during the trans-Earth flights of Apollo 15 and Apollo 16, returning from the Moon. Shown in figure 1 is a pulse-height spectrum obtained during trans-Earth flight.

Two types of data analyses were carried out: (1) Integral counts in the $\sim$ 0.6- to $\sim$ 2.7-MeV region were used to determine the

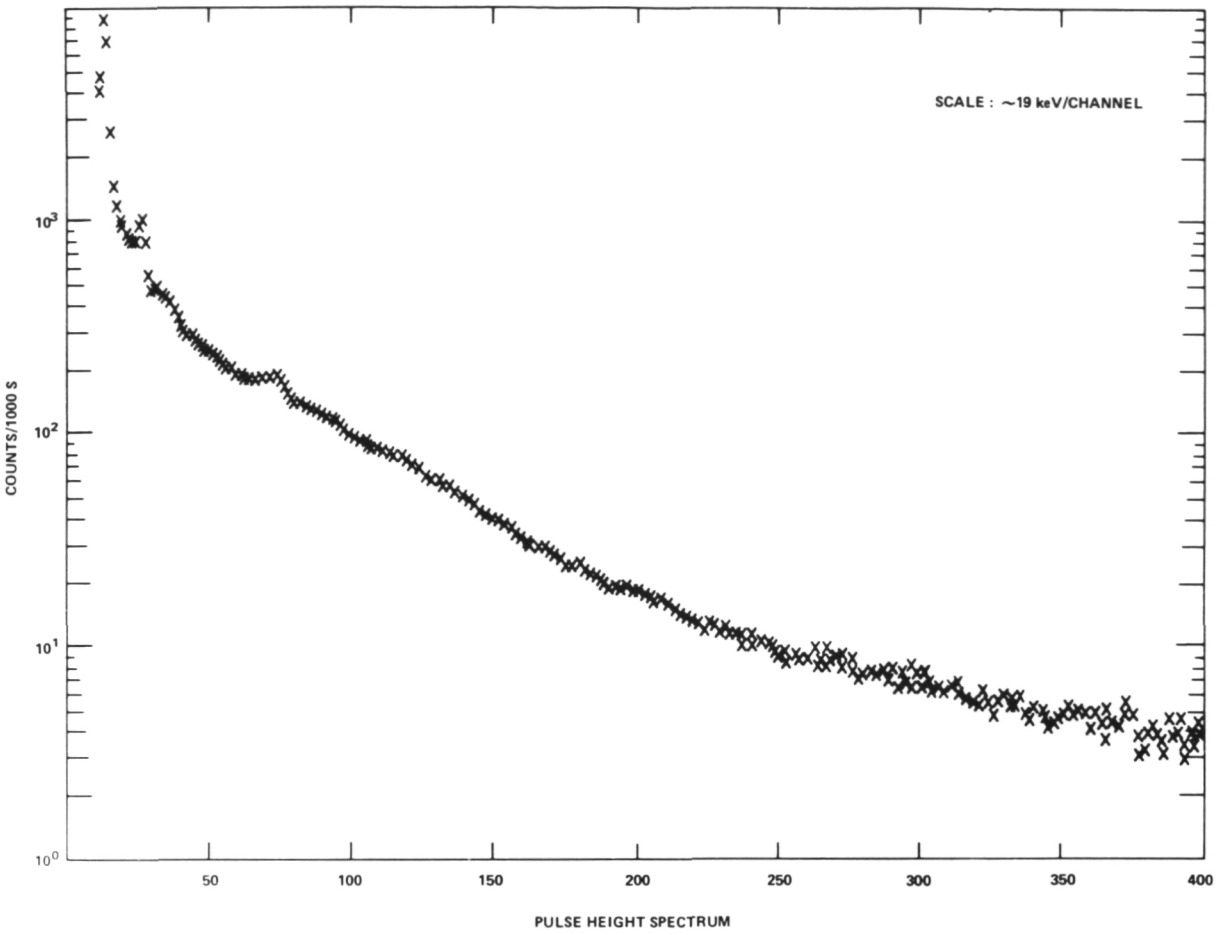

Figure 1.—*Pulse height spectrum obtained with a 7-cm by 7-cm NaI(Tl) detector, on a boom 7.6 m from the Apollo spacecraft. The measurement was made during the trans-Earth phase of the Apollo 15 mission. Scale is ~ 19 keV/channel.*

variation of the counts due to the natural emitters K, U, and Th; and (2) detailed spectral analysis was performed to separate the elemental components enabling quantitative analyses to be obtained for Th + U, K, Fe, Ti, Mg, Si, and O. With use of the methods described by Reedy, Arnold, and Trombka (ref. 3), a minimum of 30 to 40 minutes of counting was required for these quantitative analyses; for smaller data blocks, statistical errors produce unacceptable scatter. Much shorter time periods of data were used with the integral counting method for determining the natural radioactivity distribution. This integral count method works well in determining natural radioactivity. It was found that for the most part the variation in the count rate in the 0.6- to 2.7-MeV region can be attributed to gamma emission from K, Th, and U (ref. 4).

The quantitative analyses were carried out with interactive matrix inversion procedures described schematically by Reedy, Arnold, and Trombka (ref. 3). The most difficult analysis was the derivation of the lunar gamma-ray continuum, that is, the portion of the flux in the 0.5- to 10-MeV region which does not contain characteristic lines. The continuum was found to produce about 85 percent of the counts in the detector. While its general shape is understood, the continuum must be derived from the

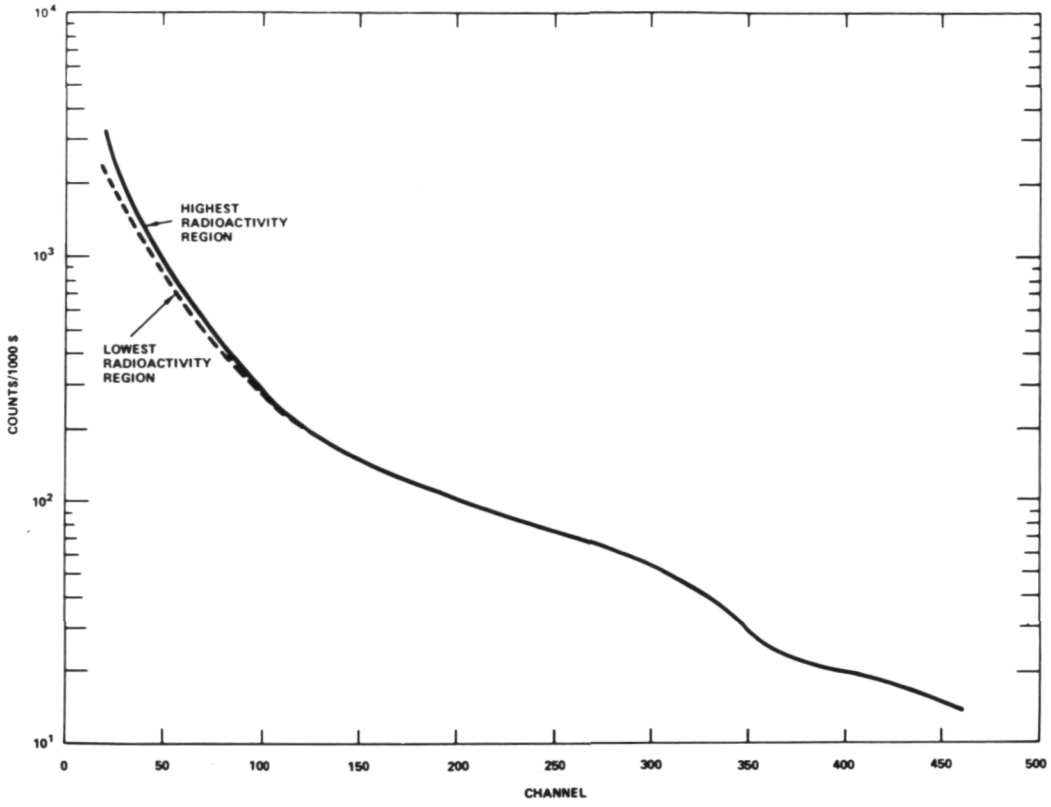

Figure 2.—*Lowest and highest background used in the analysis of the Apollo 15 lunar spectrum. Crystal detector is 7 cm by 7 cm and at a boom position 7.6 m from the spacecraft. Scale is ~ 19 keV/channel.*

data. The continuum shape and magnitude are not constant over the whole Moon. Below 3 MeV, the lines due to the radioactive elements K, Th, and U make an important contribution to this continuum by Compton scattering in the lunar material. In this manner, the continuum was separated into two components; one component was found to be constant over the lunar surface, while a second component varied as a function of the concentration of the radioactive elements K, Th, and U. The constant portion of the lunar background was derived from an analysis of lunar regions where the minimum natural radioactivity is found. The increase above this minimum level was then derived by taking differences between regions of higher activity and their low-activity regions. Empirical methods were developed to determine the magnitude and shape of the scatter

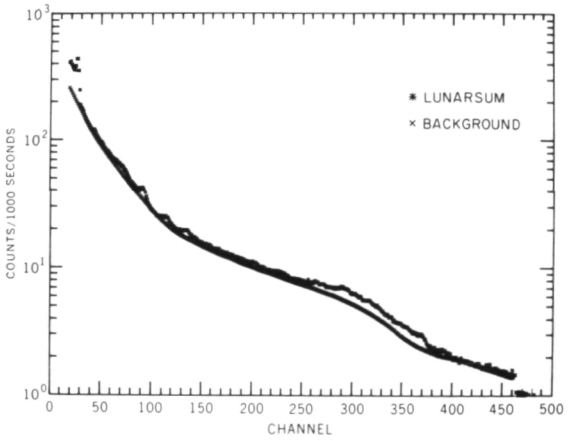

Figure 3.—*Pulse height spectrum corresponding to an average lunar spectrum for the Apollo 15 orbital mission. The derived average lunar background is also indicated. The pulse height spectra were obtained with the Apollo 15 gamma-ray spectrometer. Scale is ~ 19 keV/channel.*

buildup as a function of Th, U, and K concentration. Figure 2 shows the lowest magnitude background and the highest magnitude background used in the analysis of the Apollo 15 data. Figure 3 shows the measured lunar pulse-height spectrum obtained by integrating the spectrum over a number of hours of measurement, thus representing an average composition, over the Apollo 15 ground track and the derived lunar background for this same average spectrum. The difference pulse-height spectrum corresponding to the lunar discrete line emission pulse-height spectrum is indicated in figure 4. Also shown are the various elemental components used in the matrix analysis method (ref. 3) and the best least squares fit obtained by synthesizing these elemental components with respect to the difference spectrum.

The results to be presented in this paper were obtained from an analysis of the net discrete line spectrum from Apollo 15 and Apollo 16. The background shapes were derived from the Apollo 15 data and were used for both Apollo 15 and Apollo 16. Good agreement for elemental concentration was achieved except for the Ti calculated from the high-energy (n,γ) line in the overlap region of Apollo 15 and Apollo 16. The improved energy resolution of the Apollo 16 instrument and differences in proton-induced activation may be responsible for the changes

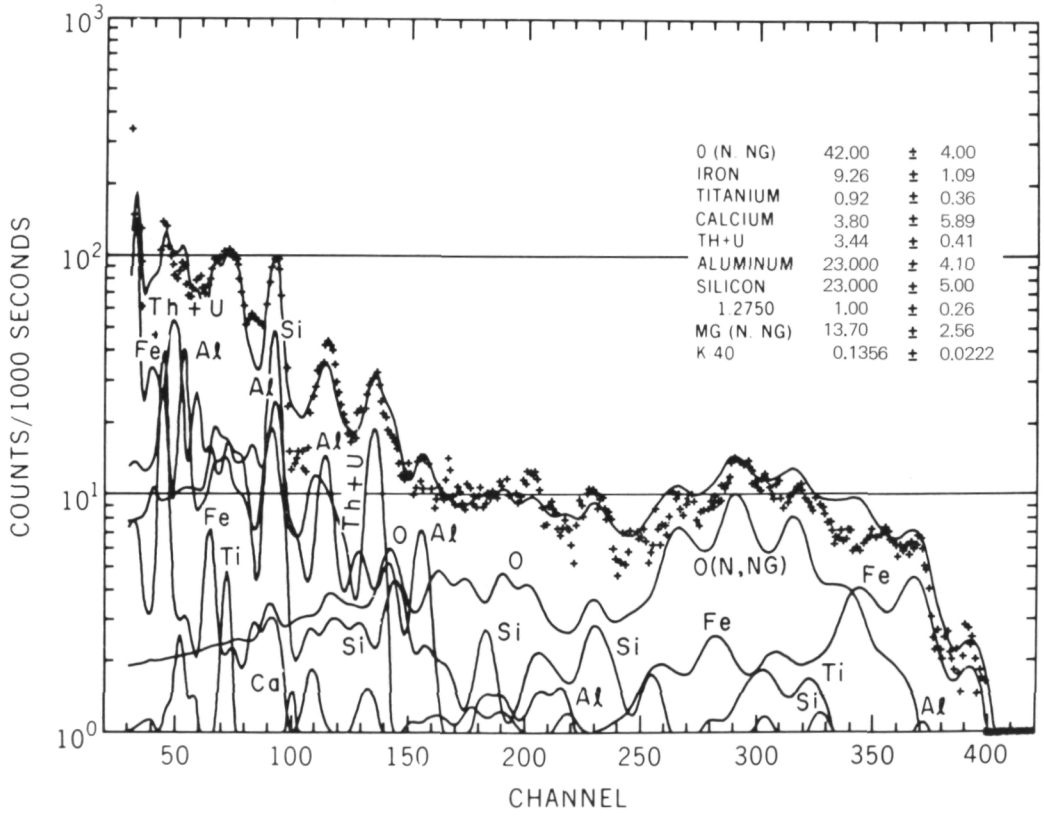

Figure 4.—*Difference pulse height spectra or discrete line lunar emission pulse height spectrum obtained with the Apollo 15 gamma-ray spectrometer over the whole ground track. The elemental components for O, Fe, Ti, Co, Th + U, Al, Si, Mg, and K are also indicated. The components were used for the least squares analysis of the difference curve. The synthesized curve obtained from least squares analysis is also shown. Scale is ~ 19 keV/channel.*

in the Apollo 16 versus Apollo 15 high-energy portion of the background which affect the Ti calculation. Separate background continua for Apollo 16 are presently being calculated.

Some changes have been made in the procedure described by Reedy, Arnold, and Trombka (ref. 3). It has been found useful to perform the analysis in two stages. In the first stage, only the spectrum from 5 to 9 MeV is analyzed; in this region, as can be seen in figure 4, only Fe, O, Si, and Ti contribute significant intensity. In the second stage of analysis, the component intensities derived by matrix inversion in stage one were subtracted from the spectrum, and all the remaining components were then used to analyze the difference spectrum in the lower energy region.

Another change in the analytical procedure involved the calculation of the iron component. Iron produces a line spectrum in the > 0.8-MeV region due to inelastic scatter of neutrons (the (n,n',γ) process), and a second line spectrum in the > 5-MeV region due to prompt capture of neutrons by the (n,γ) process. Because of the good statistics for determining the distributions for this element, the two iron components were analyzed separately. The difference in the ratio of the number flux of the (n,γ) emission with respect to the (n,n',γ) process can be used as an indicator for the presence of strong thermal neutron absorbers (such as Gd and other rare earths). This can be done because the (n,γ) gamma-ray number flux is approximately proportional to the neutron flux near thermal energies (below 1 eV). The (n,n',γ) number flux is proportional to the fast flux (above 1 MeV). Since the rare earth group includes several large thermal neutron absorbers, their presence in large concentrations will depress the magnitude of the thermal flux without significantly perturbing the fast flux. This has been seen in the analysis under consideration here. For the other elements, such as Si, which have important lines of both types, the library spectra were combined into a single component. Thorium and uranium were also combined into a single component, an estimate of the U being based on an assumption that the abundance ratio of Th/U is 3.8. This was necessary because the uranium lines, although contributing significantly to the emission spectrum, are significantly masked by other lines in the discrete line spectrum. This masking is due to the poor energy resolution of NaI (Tl) detectors. Rather precise determination of the thorium component is possible because the 2.62-MeV emission line for this element is easily discernible in the discrete line pulse-height spectra (fig. 4).

The elements which can be usefully analyzed fall into two groups. For the natural radioactivities, K and (Th + U), the elemental concentrations can be derived from the decay schemes and the properties of the detector, using theory and laboratory calibrations, with no ambiguity in principle. Concentration values for these elements were derived in this way, without adjustable parameters. The elements that depend on cosmic-ray excitation, O, Si, Fe, Mg, and Ti, require input information from nuclear and cosmic-ray physics whose combined accuracy is not yet very high. The agreement to be expected is no better than that for the parent models as proposed by Reedy and Arnold (ref. 7) for the production of cosmogenic nuclides in the Moon, and that of Lingenfelter, Canfield, and Hampel (ref. 8) for low-energy neutrons. The depth variations of induced radioactivity observed in the lunar soil are in rather good agreement (ref. 9), with Reedy and Arnold's calculations, but the absolute amounts depart by $\pm$ 25 percent from calculated values from Apollo gamma-ray data. The experiment of Woolum and Burnett (ref. 10) on Apollo 17 confirms to some extent the calculations of Lingenfelter et al. (ref. 8) of the lunar neutron flux, but suggests a somewhat harder neutron spectrum. The deviations observed from the Reedy, Arnold, and Trombka calculations (ref. 3) also suggest a harder neutron spectrum.

The best way to treat the data for O, Si, Fe, Mg, and Ti is to use "ground-truth" data,

normalizing the orbital data to the surface samples at one or more selected points. While there are many mapped areas that include several sites from which samples have been returned, most of these are unsuitable because of local variability of the soil chemistry, as, for example, the Apollo 15 landing site. The two best sites are Mare Tranquillitatis, where the Apollo 11 analyses are supplemented by the results of the Surveyor 5 experiment (ref. 11), and the Apollo 16 landing site near the Descartes region. The Apollo 15 and 16 spectrometer Fe, Mg, and Ti data were normalized to the ground-truth data for Mare Tranquillitatis, and the Descartes region ground-truth data were used as a check. Another check was performed by comparing regions overflown by both Apollo 15 and Apollo 16.

Table 1 gives the ground-truth element concentrations used for the region of Mare Tranquillitatis to derive the published values for the soil sample 10084. The exception is Ti, with a somewhat lower assumed value. The reason for this exception is that the count rates for the spectral region in which Ti is important (5.97 to 6.37 MeV) show a variation that is far outside the counting error over the Tranquillitatis region. The Apollo and Surveyor sites are in the two regions of highest observed counting rate. Because O, Si, and Fe appear to be constant in this region, the assumption is that any variation in integrated intensity is due to Ti. The conclusion drawn is that the true mean Ti concentration over the region is lower by a factor of 0.65 than that observed on the ground. This correction of course increases the uncertainty of the Ti values.

In the work to be reported, errors are not quoted because, in complex interactive analyses of the present type, the magnitude of random and systematic errors is difficult to evaluate. The main sources of error are (1) statistical counting mistakes, (2) uncertainties in the shape of the subtracted continuum, (3) unknown interactions between components, and (4) where applicable, the ground-truth normalization. At the present stage of analysis, the ground-truth comparisons and comparisons on the overlap regions of Apollo 15 and Apollo 16 give an indication of the uncertainties.

Finally, with regard to the data analysis, the compositions determined reflect the average composition down to about 20 cm in depth.

All data in table 1 (below) and in later tables are in percent or ppm element by weight. The values of Th and K are given for convenience; they are not used for renormalization. The data are for soil 10084 (refs. 12 and 13).

Table 1.—*Ground-Truth Values, Mare Tranquillitasis*

Element	Value
O	40.8%
Si	19.6%
Fe	12.1%
Mg	4.8%
Ti	2.9% (1)
Th	2.1 ppm
K	1100 ppm

NOTE: (1) This is 0.65 times the soil 10084 concentration. See text for discussion.

The X-Ray Experiment

The X-ray spectrometer consists of three large-area proportional detectors; a set of large-area filters for energy discrimination among the characteristic X-rays of Al, Si, and Mg; collimators; and data-handling electronics for obtaining eight-channel pulse-height spectra. These three detectors pointed at the lunar surface while taking measurements. A fourth proportional counter that looked in the direction opposite to the three large-area proportional counters was used as a solar monitor. The three proportional counters used to monitor the lunar X-ray flux were identical, each having an effective window area of ~ 21 cm^2. The window consisted of Be 0.0025 cm in thickness. The proportional counters were filled to a pressure of 1 atm with the standard P–10 mix-

ture of 90 percent argon (A), 9.5 percent carbon dioxide (CO_2), and 0.5 percent helium (He). To change the energy response, filters were mounted across the Be window aperture on two of the proportional counters. The filters consisted of an Mg foil (5.08×10^{-4} cm thick) and an Al foil (1.27×10^{-3} cm thick). The collimator consisted of multicellular baffles that defined a field-of-view of the three detectors to $\sim$ 44 degrees full width at half maximum. Details of the systems can be found in Adler et al. (ref. 14).

In the X-ray fluorescence experiment, the production of characteristic X-rays followed the interaction of solar X-rays with the lunar surface. The typical solar X-ray is energetically capable of producing measurable amounts of characteristic X-ray from all the abundant elements with atomic members of approximately 14 (Si) or less. The spectral characteristics and magnitude of the incident solar X-ray flux greatly affected the analysis of the data. For a detailed discussion of this problem see Adler et al. (ref. 14).

Figure 5 shows characteristic pulse-height spectra taken over Mare Crisium for the three detectors aboard Apollo 15. The spectra were normalized so that the area under the spectrum corresponding to the base detector is taken as unity. The effects of the Mg and Al filters can be seen in figures 5b and 5c. An integral count method employing the characteristics of the filters was used to determine the intensity of the characteristic lines due to Mg, Al, and Si. The relative magnitude and absolute intensity of these lines depend on the magnitude and spectral quality of the incident solar spectrum, the angle of incidence of the solar flux with respect to the look direction of the X-ray detectors, the local altitude of the detectors with respect to the lunar surface, and the surface composition and physical characteristics. If the solar spectral shape is constant, it is found that the other correction factors having to do with detector-spacecraft geometry and physical characteristics of the surface material cancel out in the calculation ratios of the abundance ratios Al/Si and Mg/Si. Further, if it is assumed that the Si concentration is constant over the lunar surface sampled (an assumption supported to good accuracy by sample analyses to date), then these ratios reflect the changes in the Al and Mg concentration over the lunar surface. Actual concentrations were obtained by an approach that is both theoretical and empirical. The theoretical calculations are based on the assumption of a quiet Sun and a coronal temperature of 4×10^6 K. These conditions give an X-ray energy distribution, consisting of both a continuum and characteristic lines, that is consistent with the solar-monitor observations. The X-ray energy distribution and various soil compositions, as determined from the analysis of lunar samples, were used to calculate a relationship between Al/Si intensity ratios as a function of chemical ratios. The empirical approach involves the assumption that the soil values from the Apollo 11 site at Mare Tranquillitatis and the Luna 16 soil values from Mare Fecunditatis are ground-truth values. With these values and the theoretically calculated slopes, values of Al/Si concentrations for

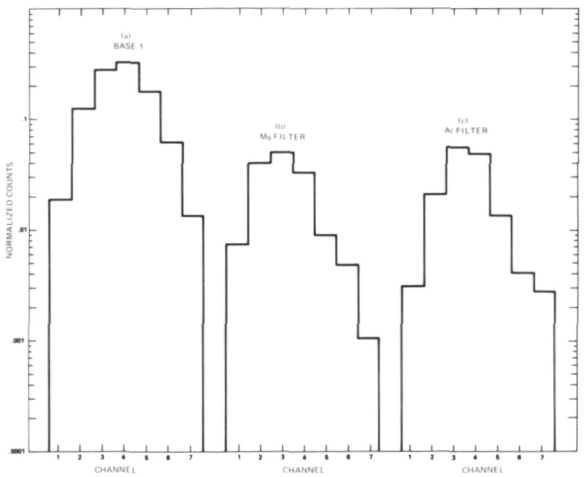

Figure 5a–c.—*Pulse height spectra obtained with the Apollo 15 X-ray spectrometer. The spectrum was taken over Mare Crisium. Spectra shown are from the base detector (a), the detector with the Mg filter (b), and the detector with the Al filter (c). The scale as shown has a lower level of 0.75 keV and is about 0.33 keV/channel. The data have been normalized so that the area under the base detector peak is unity.*

various parts of the lunar surface along the ground track were determined. The X-ray fluorescence experiment measured surface composition down to a depth of approximately 0.1 mm. Because of the gardening (mixing) of the lunar regolith by meteorite impact, no difference in composition is expected between the X-ray and gamma-ray experiments because of the different depths sampled.

The first results of the X-ray fluorescence experiments were used to map the ratios Al/Si and Mg/Si on a broad scale across the lunar surface. Recently attempts have been made (refs. 15 and 16) to prepare more detailed maps relating the X-ray results to small lunar morphological features and to various parameters independently determined, such as photogeologic observations, gravitational anomalies, and the electromagnetic sounder results.

Various methods of contouring have been considered. One approach which seems to be rather successful has been to perform trend surface studies of the lunar data (refs. 16 and 17). Surfaces described by different order polynomial expressions are fitted to the observed data by a least-squares technique. The significance of the surface is tested by statistical means. A regional model surface which is shown to be statistically valid is assumed to be the proper model for the particular region. Differences between the observed values and the model values that are statistically significant are plotted as residuals and are interpreted as local anomalies with respect to the model. It must be remembered that in all of these analyses it has been assumed that Si is constant and that the variations can be attributed to changes in either Al or Mg composition.

Experimental Results and Interpretations

GAMMA-RAY SPECTROMETER

The first results available from the gamma-ray experiment concerned the distribution of the radioactive elements of Th, U, and K (refs. 5, 18, and 19). In the spectral region above the 0.51-MeV line and up to and including the highest energy line, the 2.61-MeV line due to Th, the regional differences in count rate are overwhelmingly due to the varying intensities of the lines of Th, U, and K. This is a fortunate circumstance because the statistical precision of the total count in this region (the integrated intensities from 0.55 to 2.75 MeV) is excellent, and good area resolution can thus be obtained. In the *Proceedings of the Fourth Lunar Science Conference* (ref. 19), the count rate data are presented for 2- by 2-degree resolution elements on the lunar surface, which corresponds to a square approximately 60 km on edge. The data were adjusted to correspond to a nominal altitude of 100 km. Count rates in the energy range 0.55 to 2.75 MeV were obtained in the regions traversed by both Apollo 15 and Apollo 16, and were compared. The Apollo 16 average rate in this region is 4.6 percent greater than that from Apollo 15. This difference can be attributed to differences in particle radiation fluxes and differences in induced activity due to different trajectories through the Earth's radiation belts and the influence on Apollo 15 as compared with Apollo 16. The main results of this portion of the analysis are shown on the Moon's near and far sides, respectively.

The range of the corrected counting rates is from about 73 to 94 counts per second, or about 25 percent. The standard deviation for a typical counting time of 300 seconds per 5-degree square is about 0.5 counts per second (cps) based on counting statistics alone; it is about 1 cps for the shortest counting times used. The data from areas overflown several times on successive passes and from regions overflown on both missions provide good correlation.

The data obtained during observation periods allow some definite conclusions to be reached, even at the present early stage of data analysis.

1. On both missions, all 5-degree regions

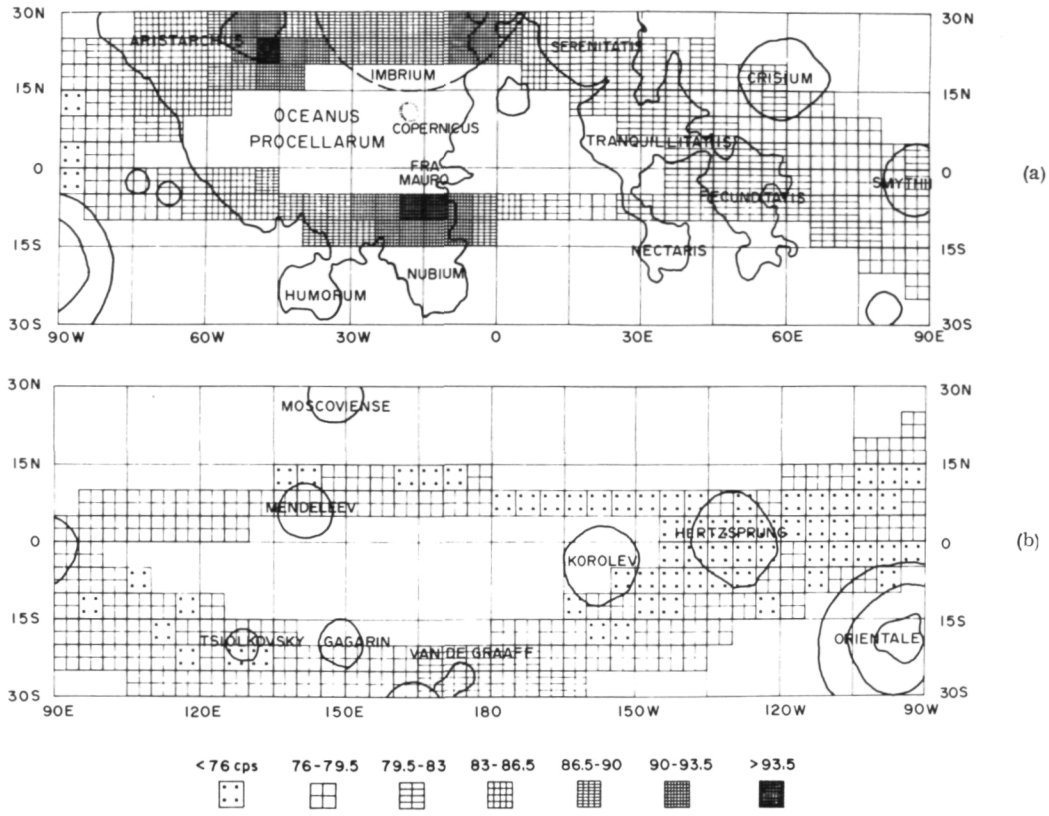

Figure 6.—*Distribution of lunar radioactivity in the energy region 0.55–2.75 MeV over the Apollo 15 and Apollo 16 ground tracks. The data are presented on a 5- by 5-degree scale over a base map freely adapted from one furnished by Dr. Farouk El Baz.*

within and bounding the overflown western maria show higher levels of radioactivity than any 5-degree region elsewhere. The contrast between this region and the rest of the observed Moon is striking, particularly as it extends to a comparison with the eastern maria. It is reasonable to infer that in most instances, the western mare regions not overflown are also highly radioactive and that other regions of the Moon are generally less radioactive. With reference to the radioactive elements, the boundaries between Oceanus Procellarum and named mare regions contiguous to Oceanus Procellarum, such as Mare Nubium, do not correspond to boundaries of composition. These observations, when combined with the radioactive content found in samples from the Apollo 12 and 14 sites (ref. 20), imply a geochemical relationship for the entire Mare Imbrium-Oceanus Procellarum Region.

2. There is detailed structure within the high-radioactivity region. The highest concentrations observed are in the Aristarchus area, in high ground west of the Apollo 15 landing site and south of Archimedes, and in the area south of the crater Fra Mauro. The Fra Mauro area overflown is about 7 degrees south of the Apollo 14 landing site, soil from which showed comparable levels of radioactive concentration. The data from this area indicate

that the Fra Mauro is, surficially at least, related to the western maria rather than the adjacent highlands as has sometimes been inferred from the albedo and topography.

3. The eastern maria show evidence of having locally enhanced radioactivity which is lower than that of the western maria. Higher intensities of radioactivity, relative to the surrounding highlands, are visible in Mare Tranquillitatis, Mare Fecunditatis, Mare Crisium, and Mare Smythii. This intensity has not been seen in Mare Serenitatis, but its accessibility to ejecta from Mare Imbrium tends to "wash out" any inherent difference. From a numerical analysis, Mare Crisium shows more contrast in radioactivity relative to its surroundings than the other eastern maria observed by the Apollo spectrometers.
4. The highland regions show low radioactivity, except on the borders of the western maria where lateral mixing seems to have occurred. On the lunar farside, the highlands to the east (180 to 90 degrees east longitude) are perceptibly more radioactive than those of the west (90 to 180 degrees west longitude) along both the Apollo 15 and 16 ground tracks. The same is true for the limb areas (compare the highland area 60 to 105 degrees east longitude to the area 90 to 120 degrees west longitude). There is a small radioactive maximum on the lunar farside near Van de Graaff (where a major magnetic anomaly is also seen); no increase is observed at these longitudes between 8 to 10 degrees north latitude.
5. Figure 7 shows a profile of the lunar topography observed below the Command Service Module (CSM) by the laser altimeter for single orbits of the Apollo 15 and 16 missions (ref. 21). Superimposed on figure 7 are points representing the relative natural radioactivity. Ignoring the region of highest radioactivity in the Mare Imbrium-Oceanus Procellarum area, a strong inverse correlation between ele-

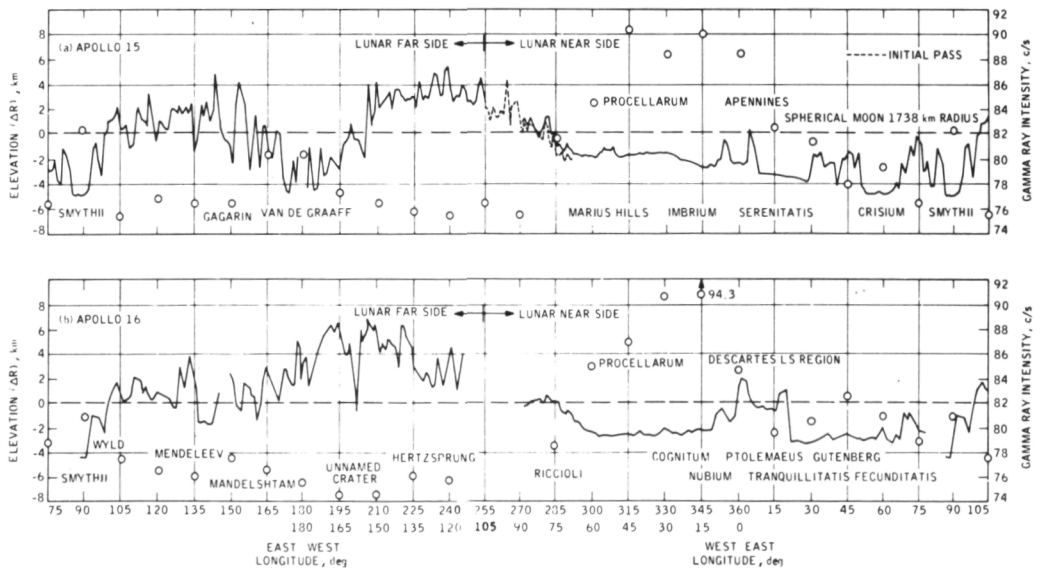

Figure 7.—*Profile of lunar topography and natural radioactivity across the Apollo 15 and Apollo 16 ground tracks as measured by the laser altimeter and gamma-ray spectrometer. The deviation is represented by the line; radioactivity plus the underlying continuum, by the points.*

vation and natural radioactivity is displayed over the remaining 360-degree track. Regions of high elevation are characterized by low material radioactivity and vice versa. While this inverse relationship is observed in the Mare Imbrium-Oceanus Procellarum region, there is structure in the radioactivity which does not correlate with changes in topography. On the lunar farside, this inverse correlation extends to an observation of greater east-west asymmetry around 180 degrees for the Apollo 16 trajectory than that of Apollo 15—an asymmetry which exists for both elevation and natural radioactivity. This inverse correlation does not appear consistently in intercomparisons among maria but rather appears to be reflecting both the nature and extent of major lunar differentiation processes. If the Moon is in isostatic equilibrium, the more extensive the early anorthositic differentiation, as characterized by lower densities and lower concentrations of the naturally radioactive nuclides than are found in mare regions, the higher the elevation and the lower the radioactivity expected.

The major lunar depression occurs in the vicinity of the crater Van de Graaff and exhibits the sharpest contrast in elevation with adjacent highlands along either ground track, that is, about 8 km. This depression

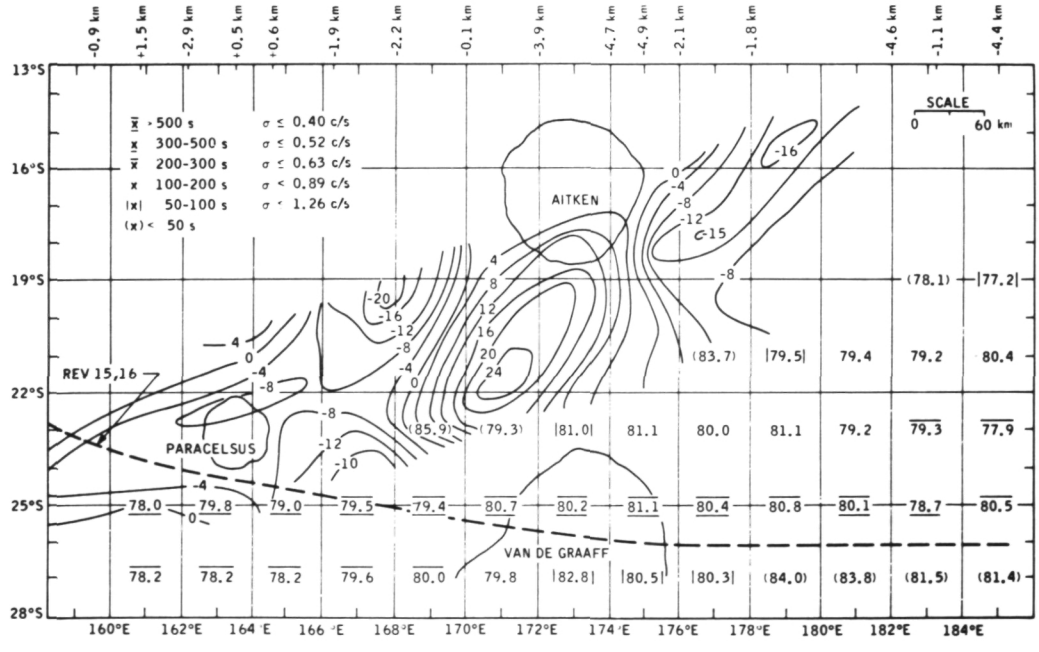

Figure 8.—*The region around the crater Van de Graaff, showing the altitude-corrected, gamma-ray intensities between 0.55 MeV and 2.75 MeV in 2- by 2-degree areas, the location of the laser altimeter ground track with elevation given at the top, and a contour map of the lunar contribution to the solar-directed component of the magnetic field from an elevation of 67 km. The subsatellite magnetometer values are in tenths of gammas. The insert gives the coding which represents the observation time within the 2- by 2-degree area, and the maximum 1σ standard deviation corresponding to that period.*

is also the site of the only major farside enhancement in natural radioactivity. The depression extends some 30 degrees in longitude on either side of 180 degrees longitude, and the gamma-ray feature is of comparable extent. Figure 8 shows the Van de Graaff area in detail. The gamma-ray intensities (counts/second) between 0.55 MeV and 2.75 MeV are calculated in 2- by 2-degree segments of area north and south of the laser altimeter track. In this case, the gamma-ray data have been corrected for spacecraft altitude but not for differences in elevation of the lunar surface. Also shown is the lunar surface magnetic field as mapped by the Apollo 15 subsatellite magnetometer with contours given in tenths of gammas (ref. 22). The elevation track is shown by the dotted line with variations from a mean radius of 1738 km tabulated at the top (ref. 21). The magnetic feature shown is the strongest observed by either the Apollo 15 or 16 subsatellite magnetometers (ref. 22). Ignoring values based on less than 50 seconds of counting time, the highest gamma-ray intensity location is identical to the minimum elevation in the Van de Graaff region. No trace of this enhanced radioactivity was found at regions north of this feature by Apollo 16. Thus, over that portion of the lunar surface scanned to date, the largest surface remanent magnetic field, one of the deepest depressions, and the only significant farside enhancement in radioactivity have all been observed within about 5 degrees (150 km) of each other. This Van de Graaff area is a notable and, to date, quite singular exception to the general conditions prevailing on the lunar farside. When understood, the area is likely to contribute significantly to comprehension of lunar evolutionary processes. This will be considered further after the following discussion of elemental composition maps.

Because of statistical problems in performing the detailed chemical analyses, the mission ground track was divided into a series of regions. Table 2 gives the number, assigned name, and lunar coordinates for each region. Figure 9 shows the actual regions in outline form. In the case of Apollo 15, the data for early revolutions have not been used in this synthesis; hence, the western portions (southwestern or northwestern in east and west longitudes, respectively, except those near 0 and 180 degrees longitude) of regions observed by Apollo 15 are heavily weighted. These regions were chosen by considering major topographic boundaries, the density of high-quality data in a given region, and the contrasts observed in the radioactivity maps (fig. 6). The smallest regions, such as Mendeleev, were chosen in order to determine the minimum area in which useful data can be derived; the errors in these regions are so large that no statistically meaningful concentrations can be derived. In this paper, the analysis used only data with sufficient total counts above background, indicating significantly low statistical errors; thus complex border regions were assigned either to mare or to highland. Doubtless, this reduced the true chemical contrasts in some regions.

Table 3 presents the results of the analysis for Apollo 15 data, normalizing Fe, Mg, and Ti as described above. The values for Fe are weighted means for the two modes of analysis. Starred values note regions where the values determined from neutron capture (low energy) are well below those from inelastic scatter (MeV neutrons). These regions appear to have high concentrations of K, Rare Earths, and P (KREEP), whose rare earth content should depress the thermal flux. In such places the true Fe content may be up to a few percent higher than shown here.

Table 4 gives the Apollo 16 results. The Apollo 15 continuum was used for this work, with very good consistency except for the Ti results, which are omitted. Here again, Fra Mauro gives evidence of a depressed thermal neutron flux; the apparent depression in a few highland regions is not yet understood.

In table 5 a number of instructive comparisons are presented. In the crossover region near the east limb, the regions analyzed on the two missions are roughly the same, and the comparison should give good agree-

Table 2.—*Lunar Regions Analyzed*

Number	Assigned Name	Coordinates Boundary Regions
	Apollo 15:	
34	Van de Graaff Region	168°W–168°E
35	Highland East Farside	168°E–82°E (south of 10°S) 168°E–88°E (north of 10°S)
36	Highland East Nearside	from (Region 35) to 60°E
37	Mare Fecunditatis	60°E–42°E
38	Mare Tranquillitatis	42°E–21°E
39	Mare Serenitatis	21°E–6°E
40	Archimedes Region	6°E–15°W
41	Mare Imbrium	15°W–39°W
42	Aristarchus Region	39°W–54°W
43	Oceanus Procellarum (north)	54°W–81°W
44	Highland West Farside	81°W–168°W
	Apollo 16:	
26	Highland East Farside	180°–142°E
22	Mendeleev	142°E–138°E
28	Highland East Limb	138°E–92°E
20	Mare Smythii	92°E–83°E
19	Highland East Nearside	83°E–55°E
17	Mare Fecunditatis	55°E–44°E
14	Intermediate Mare-Eastern Highland	44°E–21°E
12	Highland Nearside Center	21°E–5°E
10	Ptolemaeus-Albategnius	5°E–5°W
23	Fra Mauro Region	5°W–20°W
8	Mare Cognitum	20°W–30°W
5	Oceanus Procellarum (south)	30°W–50°W
3	Grimaldi Region	50°W–76°W
2	Orientale Rings	76°W–105°W
29	Highland West Limb	105°W–119°W
1	Hertzsprung Region	119°W–136°W
27	Highland West Farside	136°W–180°

ment. The highland region from 5 to 21 degrees east longitude, which includes the Descartes region, is compared with the soil analysis. The deviations seen are in the expected direction if more mare and KREEP materials are mixed in near the margins of the region.

A plausible comparison is possible at two landing sites that were not overflown. Apollo 14 observed the northern end of the Fra Mauro formation; Apollo 16 overflew the southern end. Whatever the origin of this feature, similarities are to be expected throughout. Apollo 12 sampled an area of Oceanus Procellarum not very far from, and topographically similar to, the area overflown by Apollo 16. These comparisons are shown in parts (c) and (d) of table 5.

All these comparisons seem generally satisfactory and serve to confirm the validity of the analysis. There is room for further work in a number of areas and this in underway. However, no substantial modification of the values reported here is expected.

An implication of the results just obtained is that the contrasts between mare and high-

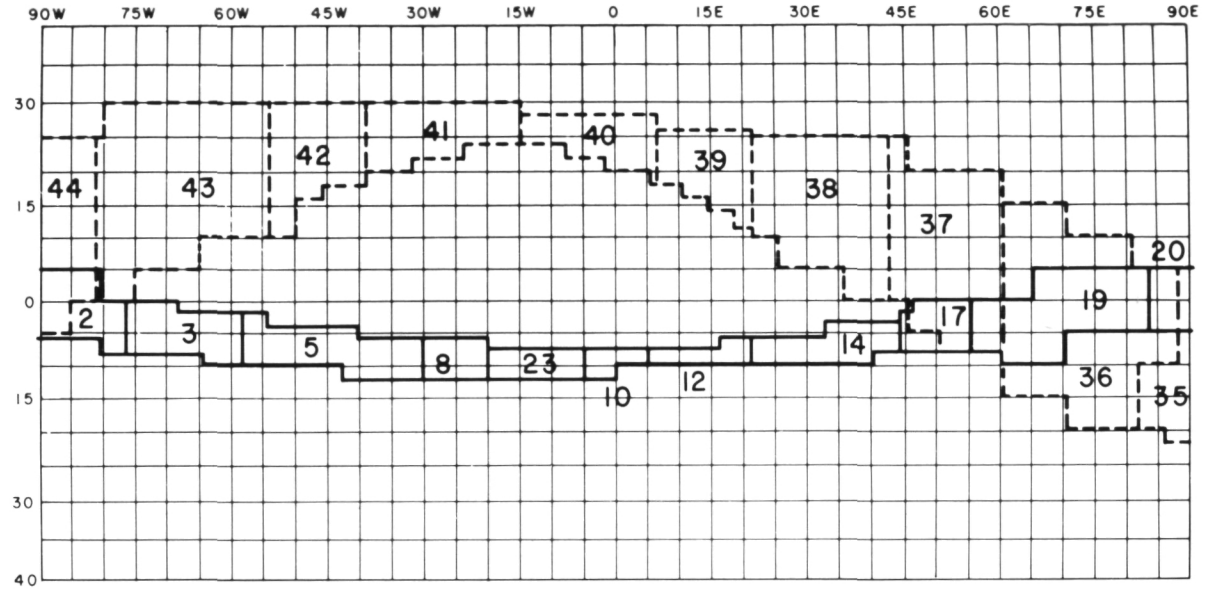

LUNAR NEAR SIDE

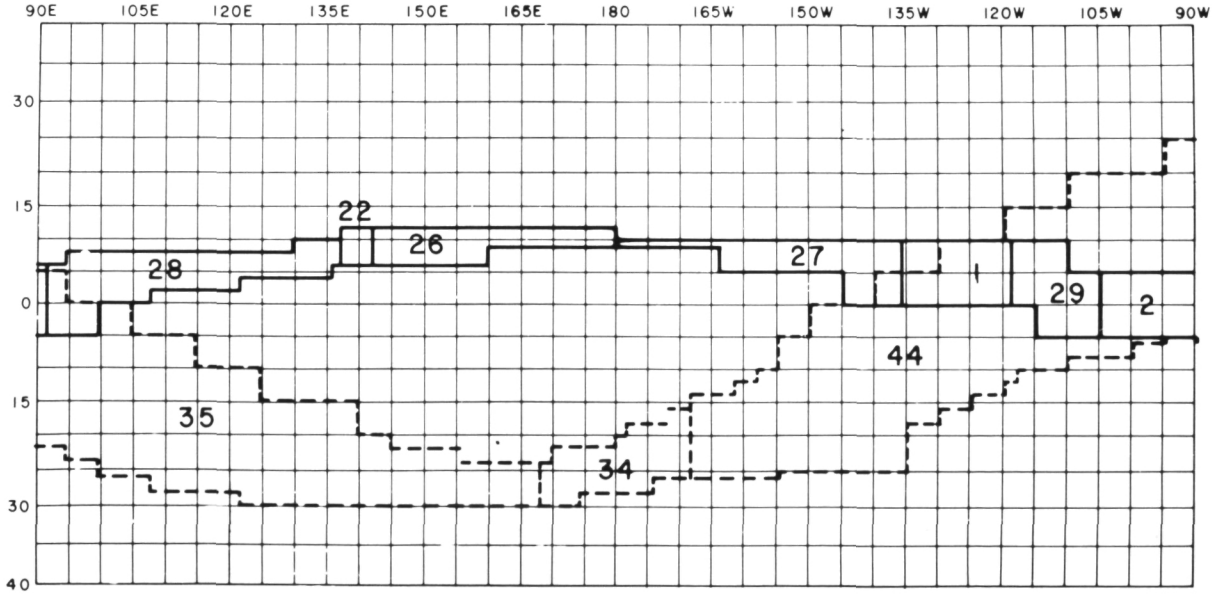

LUNAR FAR SIDE

Figure 9.—*Areas on the Moon used in the lunar data analysis (see table 2 for key).*

Table 3.—*Apollo 15: Element Concentrations by Regions*

Region	Fe(%)	Mg(%)	Ti(%)	Th(ppm)	K(ppm)
34	7.7	3.8	0.1	2.3	1600
35	6.5	4.5	1.3	1.0	940
36	9.3	5.7	0.8	1.4	1200
37	11.3	7.0	2.2	1.2	1400
38 [1]	(12.1)	(4.8)	(2.9)	1.7	1200
39	10.7	6.6	2.6	2.3	1700
40	8.4 [2]	6.3	0.8	6.8	3100
41	13.6	6.2	1.4	5.8	1700
42	9.6 [2]	4.9	2.2	6.9	2500
43	10.5	4.6	2.0	3.9	1700
44	5.7	3.5	1.5	0.4	950
All Data	8.7	4.8	1.45	2.2	1230

NOTES: (1) Values in parentheses are ground-truth data used to normalize concentrations for these elements in all regions.
(2) Region of apparent depressed thermal neutron flux (see text).

Table 4.—*Apollo 16: Element Concentrations by Regions*

Region	Fe(%)	Mg(%)	Th(ppm)	K(ppm)
26	6.2	3.4	0.6	920
22	4.3	3.0	0.5	960
28	7.2	2.9	0.5	840
20	8.8	2.8	1.3	1900
19	8.6	4.5	1.3	980
17	9.0	4.6	2.1	1100
14	9.0	3.5	1.5	1300
12	5.9	4.0	2.1	1400
10	4.8 [1]	5.2	5.0	2700
23	9.7 [1]	5.7	10.5	3900
8	12.1	4.9	8.4	3600
5	12.2	5.0	5.0	2300
3	4.4 [1]	3.6	2.4	1100
2	4.7	2.9	0.8	1000
29	3.5 [1]	2.1	0.4	1200
1	3.6 [1]	3.6	0.6	720
27	5.2	2.7	0.5	730
All Data	7.2	3.6	2.1	1300

NOTE: (1) Region of apparent depressed thermal neutron flux (see text).

land regions are as expected nearly everywhere. In the maria, Fe (and, less strikingly, Mg) is relatively enriched. The radioactive elements show the same pattern except for one place.

The Van de Graaff region (table 3, Region 34) shows a chemical composition different from any thus far observed on the Moon. The major elements are highland-like, though Fe content is a little high for this. The concentrations of K and Th are very similar to those of Mare Tranquillitatis and are typical for a mare. The Ti concentration is significantly below that of any region analyzed. Such a composition could not be formed by mixing the major components as observed elsewhere.

The most exciting possibility concerning the composition of the remarkable "granitic" rock 12013 is that Van de Graaff or some chemically similar unmapped region is its source. The K/Th ratios are compatible (ref. 25) and about 5 percent of material of 12013 chemistry, added to highland soil, could produce the observed radioactivity. The major elements are also compatible, though this is not a useful check at the 5-percent level. The Van de Graaff region is very far from all the landing sites; it is thus expected that such material would be uncommon among the returned samples.

The large highland regions are not entirely uniform. Most notable is an east-west asymmetry in the lunar farside. The iron concentration is higher in the eastern regions, which are lower topographically (ref. 21), and this effect extends to the limb and near to the mare edges. The radioactivity

Table 5.—*Comparisons of Orbital Data with Returned Lunar Samples*

Some Comparisons

	a. East Crossover		b. Ground Truth	
	Apollo 15 Region 36	Apollo 16 Region 19	Apollo 16 Region 12	Descartes Soil [3]
Fe(%)	9.3	8.6	5.9	4.0
Mg(%)	5.7	4.5	4.0	3.3
Th(ppm)	1.4	1.3	2.1	2.0
K(ppm)	1200.	980.	1400.	940.

Ground Analogies

	c. Fra Mauro		d. Oceanus Procellarum	
	Apollo 16 Region 23	Apollo 14 Soil [2]	Apollo 16 Region 5	Apollo 12 Soil [3]
Fe(%)	9.7	8.1	12.2	12.5
Mg(%)	5.7	5.6	5.0	6.2
Th(ppm)	10.5	11.6	5.0	7.6
K(ppm)	3900.	4400.	2300.	2600.

NOTES: (1) Fe and Mg: Average of soil analysis, taken from five papers, Third Lunar Science Conference and PET report. K and Th from Eldridge et al. (ref. 23).

(2) Fe and Mg: Average of soil analysis, taken from five papers, Third Lunar Science Conference, and PET report. K and Th from Eldridge et al. (ref. 24).

(3) Fe and Mg: Average of analyses of bulk soil 12070 and related samples in five papers, Second Lunar Science Conference. K and Th from O'Kelley et al. (ref. 25).

maps show more detail (fig. 6). The dry basins like Mendeleev give typical highland analyses within a rather large experimental error.

The values of Ti found in the farside highlands from Apollo 15 data are unexpectedly high and are another example of inhomogeneity in broad highland areas.

There are also differences among maria and KREEP-rich regions. The variability in Ti has been well documented in the mare samples and is well displayed in the comparison of Mare Imbrium (Region 41) with Oceanus Procellarum (Region 43). The Archimedes and Aristarchus regions also differ in Ti and probably in Fe.

The most interesting element ratio is K/Th (and its assumed close correlate K/U). In both missions this ratio rises from something like 400 in the KREEP-rich regions to ratios of 1000–2000 in the highlands. Figure 10 shows plots of the two-element concentrations for the two Apollo missions (15 and 16), as a function of longitude. The errors for both elements are of course larger at the lowest concentrations, but the trend is unmistakable.

Earlier, interpretations of radioactivity maps were presented in terms of a three-component model: mare basalt, KREEP, and a low-radioactivity highland component (ref. 6). Clearly, this preliminary model is inadequate for the detailed information now available, as evidenced at Van de Graaff, where material not prominently displayed in lunar samples so far described is observed. However, no broad regions dominated by radically different chemistry (basic rocks or granites) are observed in the present analysis. If such regions exist, they lie in areas so far unmapped.

X-RAY SPECTROMETER

With the gamma-ray spectrometer results in mind, the results of the X-ray spectrometer are summarized (refs. 14–17, and 26–28). These results will add Al to the elemental composition obtained with the gamma-ray spectrometer. Furthermore, much more detailed information on areal distribution for both Al and Mg is obtainable because of the superior spatial resolution of the X-ray detector.

Figures 11a, 11b, 12a, and 12b show Al/Si and Mg/Si profiles along a northern and a southern track observed by the Apollo 15 mission. Figures 13a and 13b show the Al/Si profile along a track of the Apollo 16 mission. Because of the greater area covered by Apollo 15, two paths for the Apollo 15 mission are included.

The method of calculation of the Al/Si

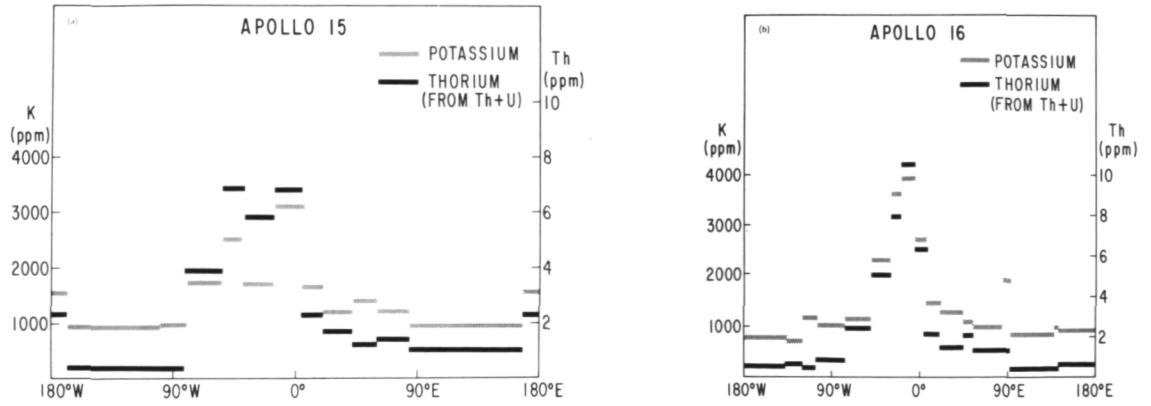

Figure 10.—*(a) Potassium and thorium on the lunar surface, plotted against longitude on the Apollo 15 ground track. (b) A similar plot for Apollo 16, with different thorium scale.*

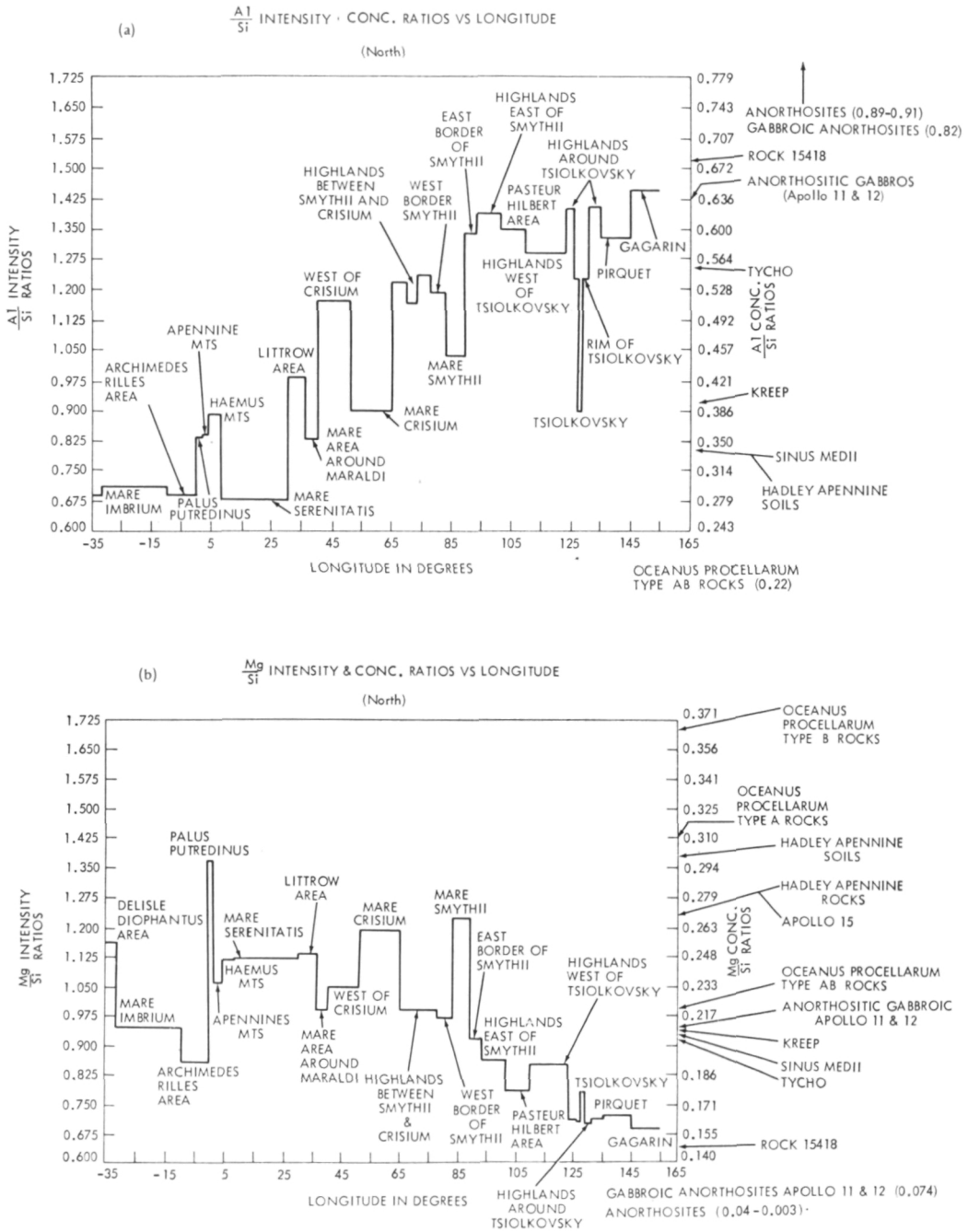

Figure 11.—*(a) Al/Si ratio versus longitude for the Apollo 15 ground northern track. The values for some reference material are shown. (b) Mg/Si ratios for the same tracks as northerly track above.*

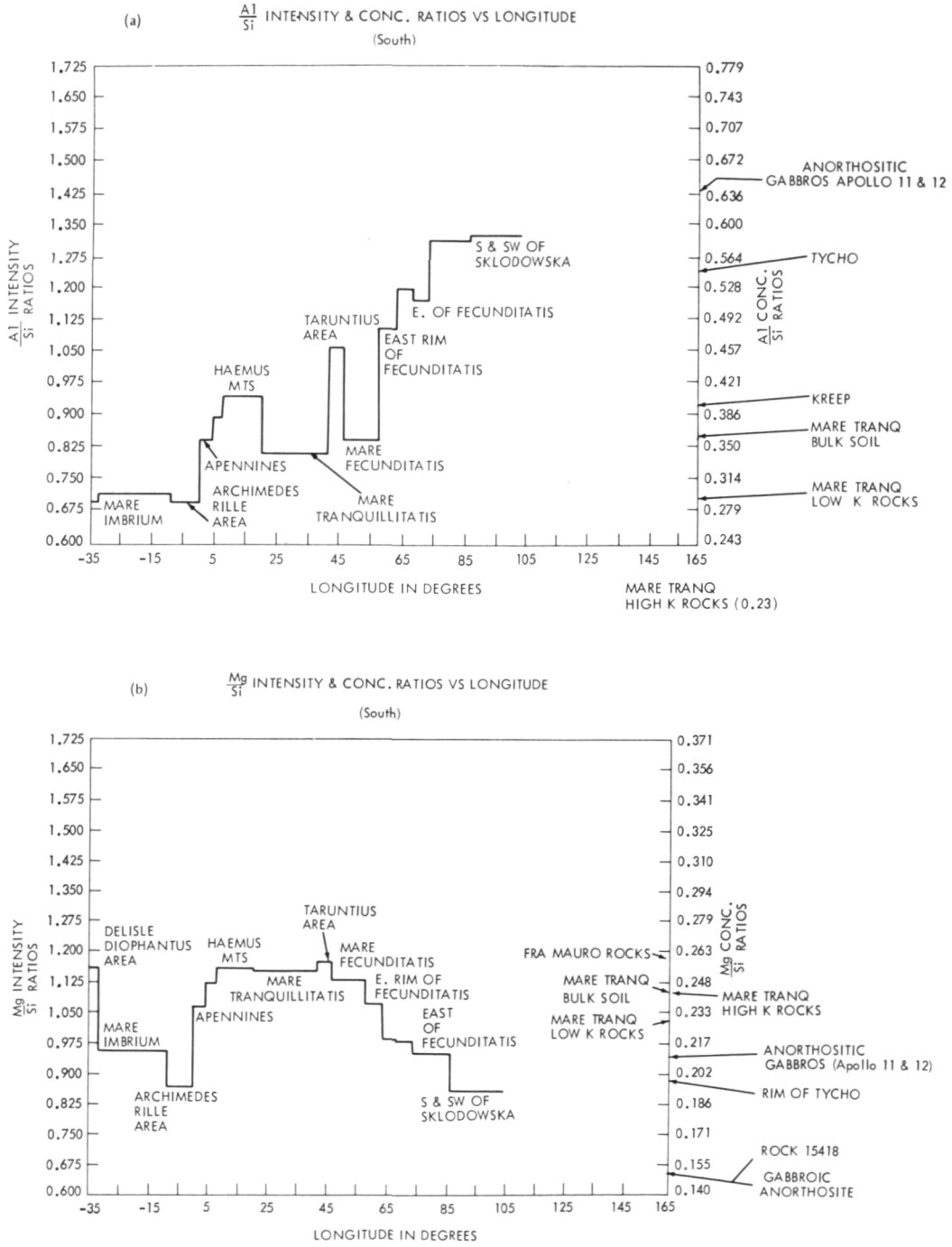

Figure 12.—*(a) Al/Si for the Apollo 15 southern ground track; (b) Mg/Si for the same southern track.*

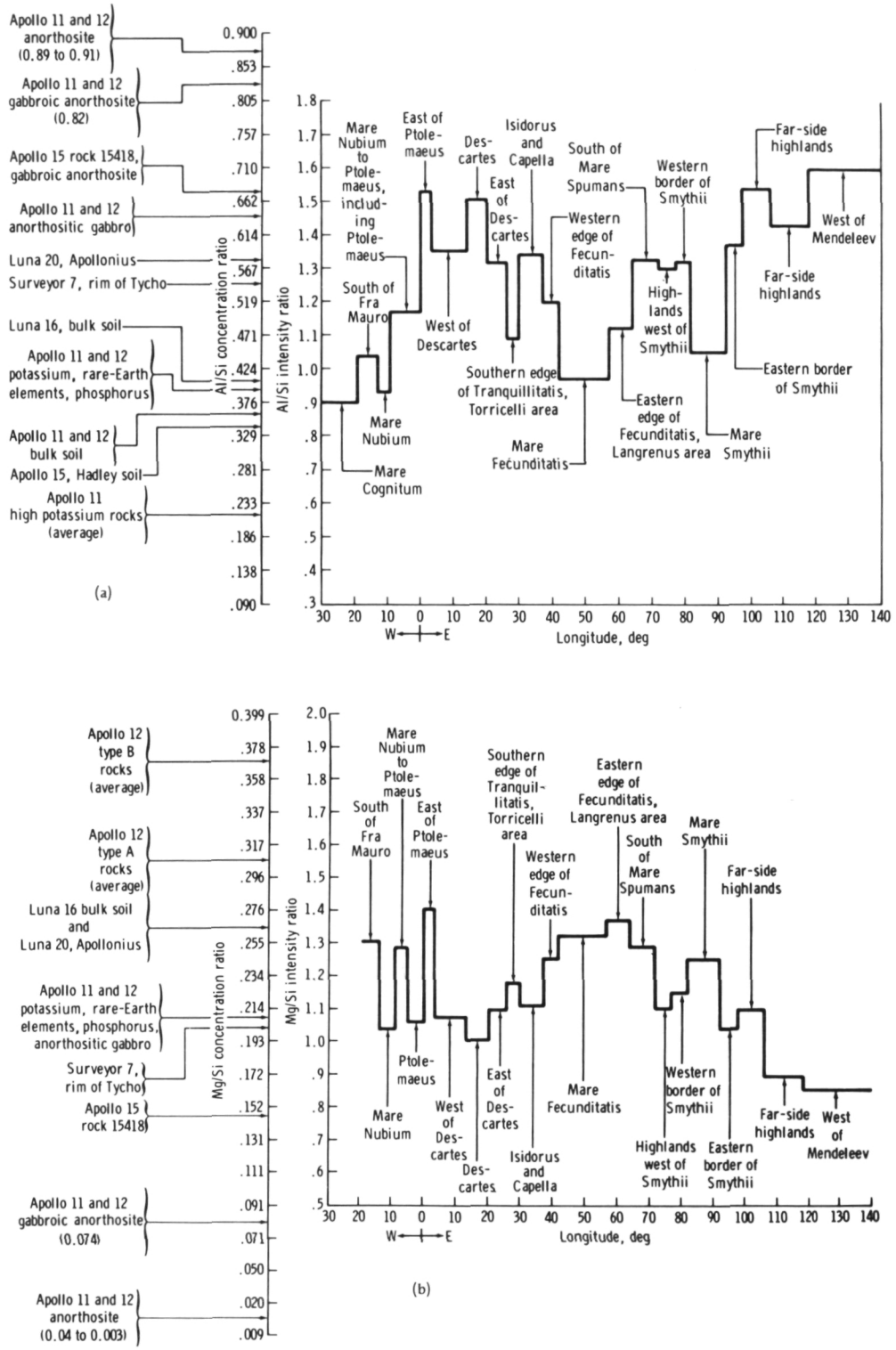

Figure 13.—*(a) Al/Si for the Apollo 16 ground track; (b) Mg/Si for the same track.*

and Mg/Si concentration ratios was previously discussed, and the results are shown in tables 6, 7, and 8. Table 6 shows the consistency in measurement between the Apollo missions. Tables 7 and 8 give results obtained over a number of lunar features. The results are obtained by integrating the spectra obtained through a number of passes over the same feature.

The data show some striking regularities:

1. The Al/Si ratios are highest in the eastern limb highlands and considerably lower in the mare areas. The extreme variation is about a factor of 2, the lowest value occurring in the Imbrium basin region. The Mg/Si concentration ratios generally show the opposite relationship. If the gamma-ray results reported above for the Fe concentration are considered, it is found that Fe is high, in low-Al regions, and the converse is also found. Also, in those regions where the Mg does remain constant, in comparison with the spatial resolution of the gamma-ray detector, there is good agreement between Mg/Si concentrations calculated from the X-ray and gamma-ray measurements. The Al/Si and Mg/Si chemical ratios for the highlands correspond to that for anorthositic gabbro through gabbroic anorthosites or feldspathic basalts. By contrast, the chemical ratios for the mare areas correspond to the mare basalts. This result is consistent with the gamma-ray results on Fe, Th, U, and K reported above.
2. Our early reports (while the Apollo 16 mission was in progress) of very high Al/Si ratios in the Descartes area were confirmed by the analysis of the lunar samples brought back from the site. The values reported of 26.5 percent aluminum oxide agree very well with the estimates in table 6. It appears reasonable from the data that some material sampled at Descartes is similar to that of the eastern limb and farside highlands. This conclusion is further justified by the fact the Mg/Si concentration ratios for some of the returned materials is about 0.18, close to the values reported here of 0.19 ± 0.05. The eastern limb highlands and farside highlands as shown in table 6, are about 0.16 to 0.21.
3. In both Apollo 15 and Apollo 16 missions, the Al and Mg values derived show an inverse relationship in most instances. The inverse relationship between Al obtained from the X-ray results and Fe obtained from the gamma-ray results is even more striking.
4. There are distinct chemical contrasts

Table 6.—*Comparison of Overlap Between Apollo 15 and Apollo 16 Ground Tracks*

Feature (1)	Apollo 16 Concentration Ratio		Apollo 15 Concentration Ratio	
	Al/Si $\pm$ 1σ	Mg/Si $\pm$ 1σ	Al/Si $\pm$ 1σ	Mg/Si $\pm$ 1σ
Mare Fecunditatis	0.41 $\pm$ 0.05	0.26 $\pm$ 0.05	0.36 $\pm$ 0.06	0.25 $\pm$ 0.03
Mare Smythii	0.45 $\pm$ 0.08	0.25 $\pm$ 0.05	0.45 $\pm$ 0.06	0.27 $\pm$ 0.06
Langrenus area	0.48 $\pm$ 0.07	0.27 $\pm$ 0.06	0.48 $\pm$ 0.11	0.24 $\pm$ 0.06
Highlands west of Smythii	0.57 $\pm$ 0.07	0.21 $\pm$ 0.03	0.55 $\pm$ 0.06	0.22 $\pm$ 0.03
Western border of Smythii	0.58 $\pm$ 0.08	0.22 $\pm$ 0.04	0.52 $\pm$ 0.06	0.22 $\pm$ 0.06
Eastern border of Smythii	0.61 $\pm$ 0.09	0.20 $\pm$ 0.06	0.60 $\pm$ 0.10	0.21 $\pm$ 0.03

NOTE: (1) The overlap between corresponding areas of the Apollo 16 and 15 ground tracks is not exact, and therefore differences for the same area may be real.

Table 7.—*Concentration Ratios of Al/Si and Mg/Si for the Various Features Overflown During Apollo 15 Mission*

Feature	Concentration Ratios	
	Al/Si ± 1σ	Mg/Si ± 1σ
West of Diophantus and Delisle,	0.26 ± 0.13	0.21 ± 0.06
northeast of Schröters Valley	0.28 ± 0.08	0.21 ± 0.06
Mare Serenitatis	0.29 ± 0.10	0.26 ± 0.07
Diophantus and Delisle area	0.29 ± 0.08	0.19 ± 0.05
Archimedes Rille area	0.30 ± 0.10	0.21 ± 0.06
Mare Imbrium	0.34 ± 0.06	0.25 ± 0.04
Mare Tranquillitatis	0.35 ± 0.08	0.22 ± 0.04
Mare east of Littrow (Maraldi)	0.35 ± 0.09	0.30 ± 0.03
Palus Putredinus	0.36 ± 0.06	0.25 ± 0.03
Mare Fecunditatis	0.36 ± 0.09	0.23 ± 0.05
Apennine Mountains		
Haemus Mountains, west border of	0.38 ± 0.10	0.25 ± 0.05
Serenitatis	0.39 ± 0.08	0.26 ± 0.05
Mare Crisium	0.39 ± 0.11	0.18 ± 0.02
Tsiolkovsky		
Haemus Mountains, south-south-	0.40 ± 0.07	0.26 ± 0.04
west of Serenitatis	0.42 ± 0.10	0.25 ± 0.06
Littrow area	0.45 ± 0.06	0.27 ± 0.06
Mare Smythii		
Taruntius area, between Tranquillitatis and Fecunditatis	0.45 ± 0.07	0.26 ± 0.02
Langrenus area, east of Fecunditatis to 62.5°E	0.48 ± 0.11	0.24 ± 0.06
Highlands between Crisium and Smythii (Mare Spumans and Mare Undarum area)	0.51 ± 0.06	0.22 ± 0.05
Highlands east of Fecunditatis,	0.51 ± 0.10	0.22 ± 0.05
Kapteyn area 68°–73°E 7.5°–15°S	0.51 ± 0.10	0.23 ± 0.05
Highlands west of Crisium		
Highlands east of Fecunditatis 62.5°–68°E, 4°–12.5°S	0.52 ± 0.10	0.22 ± 0.05
West border of Smythii to 4°–5° out from Rim	0.52 ± 0.06	0.22 ± 0.03
South of Crisium, Apollonius area, to Fecunditatis, 50°–60°E	0.53 ± 0.06	0.23 ± 0.03
East border of Crisium out to 6° from Rim	0.54 ± 0.09	0.22 ± 0.04
	0.54 ± 0.12	0.16 ± 0.02
Tsiolkovsky—Rim		
Highlands between Crisium and Smythii, 2.5°S 69°E, 5°S 76°E, 12°N 80°E, 10°N 83°E	0.55 ± 0.06	0.22 ± 0.03
Highlands west of Tsiolkovsky, 110°–124°E to 9°–21°S	0.57 ± 0.11	0.19 ± 0.04
Highlands east of Fecunditatis 73°–85°E, 10°–19°S	0.58 ± 0.13	0.21 ± 0.05
South and southwest of Sklodowska,	0.59 ± 0.14	0.19 ± 0.07
86°–101°E, 18°–23°S	0.59 ± 0.15	0.16 ± 0.05
Pirquet, 135°–145°E, 18°–23°S	0.60 ± 0.10	0.21 ± 0.03
East border of Smythii, out to 4°–5°		
Pasteur Hilbert highlands area, 101.5°–110°E, 7°–18°S	0.60 ± 0.10	0.18 ± 0.04
Hirayama, highlands east of Smythii, 89°E 12°S,	0.62 ± 0.07	0.19 ± 0.04
100°E 15°S, 98°E 2°S, 103°E 5°S	0.62 ± 0.12	0.15 ± 0.06
Highlands around Tsiolkovsky		
South part of Gagarin, 144°–153°E, 21°–23°S	0.65 ± 0.24	0.14 ± 0.05

Table 8.—*Concentration Ratios of Al/Si and Mg/Si for the Various Features Overflown During Apollo 16 Mission*

Feature	Concentration Ratios	
	Al/Si ± 1σ	Mg/Si ± 1σ
Mare Cognitum	0.38 ± 0.11	0.40 ± 0.29
Upper part of Sea of Clouds, 9°–13°W	0.39 ± 0.12	0.20 ± 0.05
Mare Fecunditatis, 42°–57°E	0.41 ± 0.05	0.26 ± 0.05
South of Fra Mauro, 13°–19°W	0.45 ± 0.07	0.26 ± 0.04
Mare Smythii, 82°–92.5°E	0.45 ± 0.08	0.25 ± 0.05
Southern edge of Mare Tranquillitatis, Torricelli area, 26°–30°E	0.47 ± 0.09	0.23 ± 0.05
Eastern edge of Fecunditatis, Langrenus area, 57°–64°E	0.48 ± 0.07	0.27 ± 0.06
Ptolemaeus, 4°W–0.5°E	0.51 ± 0.07	0.21 ± 0.04
Highlands west of Ptolemaeus to Mare Nubium, 4°–9°W	0.51 ± 0.11	0.25 ± 0.12
Highlands west of Mare Fecunditatis, 37.5°–42°E	0.52 ± 0.07	0.24 ± 0.05
Highlands west of Smythii, 72°–77°E	0.57 ± 0.07	0.21 ± 0.03
Western border of Smythii, 77°–82°E	0.58 ± 0.08	0.22 ± 0.04
Highlands east of Descartes, 20.5°–26°E	0.58 ± 0.07	0.21 ± 0.04
South of Mare Spumans, 64°–72°E	0.58 ± 0.07	0.25 ± 0.04
Isidorus and Capella, 30°–37.5°E	0.59 ± 0.11	0.21 ± 0.05
Highlands west of Descartes, 3°–14°E	0.59 ± 0.11	0.21 ± 0.05
Eastern border of Mare Smythii, 92.5°–97.5°E	0.61 ± 0.09	0.20 ± 0.06
Farside highlands, 106°–118°E	0.63 ± 0.08	0.16 ± 0.05
Descartes area, highlands, Apollo 16 landing site, 14°–20.5°E	0.67 ± 0.11	0.19 ± 0.05
East of Ptolemaeus, 0.5°–3°E	0.68 ± 0.14	0.28 ± 0.09
Highlands, 97.5°–106°E	0.68 ± 0.11	0.21 ± 0.05
Farside highlands west of Mendeleev, 118°–141°E	0.71 ± 0.11	0.16 ± 0.04

between such features as the small mare basins and the highland rims (note, for example, the crater Tsiolkovsky in figures 11a and 11b).

An interesting use of the data was to compare the Al/Si intensity ratios to optical albedo values. These observations are particularly significant in view of the longstanding discussions about whether these albedo differences represent topographic differences solely or also reflect compositional differences among surface materials. Early workers such as Whitaker (ref. 29) and others recognized convincing evidence for compositional changes where sharp albedo changes occur. However, it remained for the later Surveyor, Apollo, Luna, and Lunokhod missions to provide quantitive compositional data. Chemical differences related to albedo variations were first confirmed by the alpha backscattering experiment carried on Surveyors 5, 6, and 7 (ref. 30). The Surveyor 5 and Surveyor 6 experiment data were used to analyze widely separated mare sites, and chemically similar surface materials in each site were reported. The Surveyor 7 experiment, on the other hand, observed a highland site and data analysis found a significant chemical difference between that region and the two mare locations. The Surveyor results and the analyses of returned lunar samples confirmed that albedo is indeed affected by composition as well as topographic differerences. The X-ray fluorescence experiments on Apollo 15 and Apollo 16 now have provided the data for correlation of regional albedo with surface composition for these selected chemical elements.

The data from both Apollo flights exhibit an excellent correspondence between Al/Si values and the optical albedo values. An ex-

ample from the Apollo 16 flight is shown in figure 14. There is positive correlation between the albedo and the Al/Si values, although the rate of change is not always similar. In the Apollo 15 data, the main anomalies were observed where an occasional small Copernican-type crater occurred and produced an abnormally high albedo value. This was considered to be due to the highly reflective, finely divided ejecta rather than to compositional changes. A similar anomaly is noted in the Apollo 16 data around 27 degrees west longitude in a Tranquillitatis embayment north of Theophilus. Four Apollo 16 orbits are plotted. Orbits 58 and 60 show the expected decrease in Al/Si with decreasing albedo. Orbits 55 and 59, on the other hand, show an occasional increase in Al/Si although the albedo decreases. This may record the existence of an old "weathered" ray consisting of aluminum-rich, highland-derived ray material which has lost its high reflectivity. This loss is thus attributed to chemical rather than physical change.

The X-ray fluorescence experiment is especially well suited to look at the problem of horizontal transport and, particularly, the question of whether or not the mare fill is highland material carried by electrostatic forces. To appreciate this, one must keep in

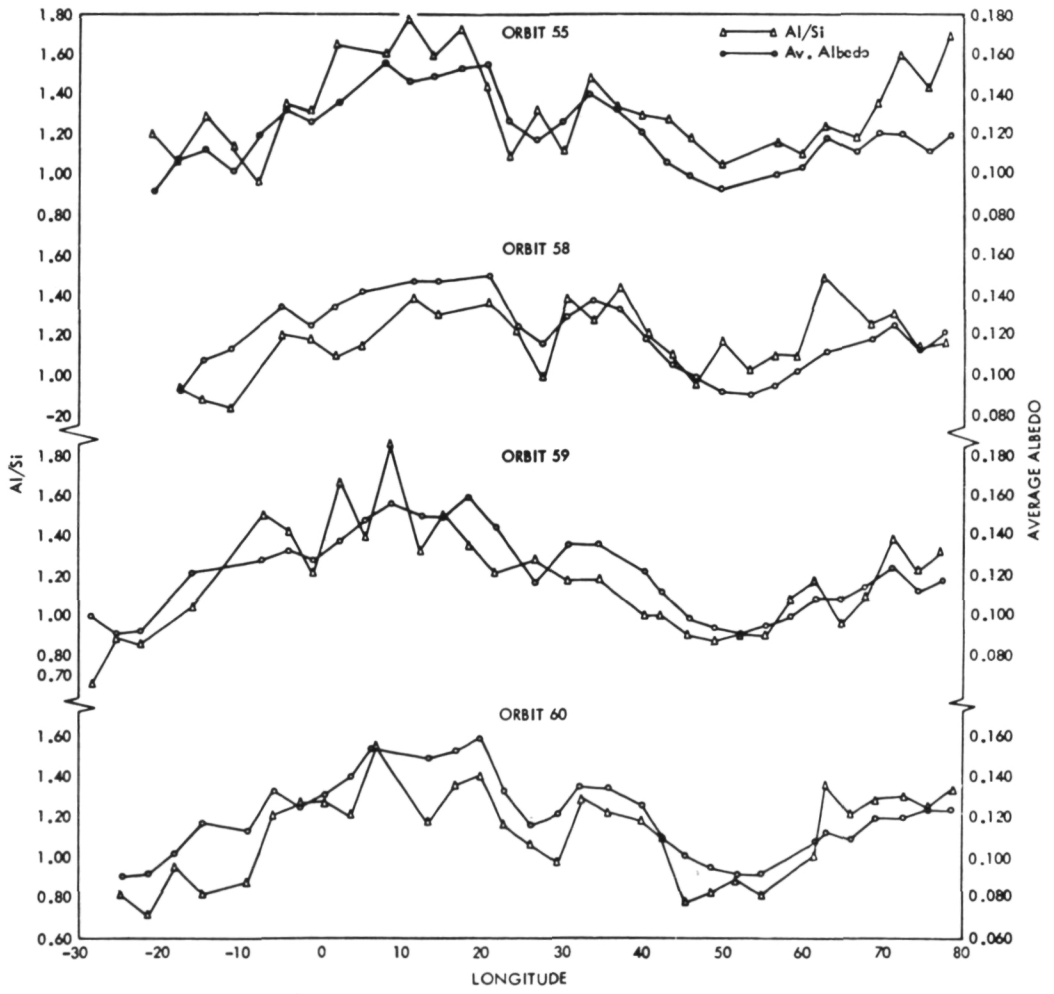

Figure 14.—*A comparison of Al/Si intensity ratios versus optional albedo values for various Apollo 16 orbits.*

mind that the X-ray measurements are extremely shallow. A 0.1-mm layer of basalt or feldspar would represent effectively infinite thickness. This is equivalent to about 3×10^{-4} g/cm^2 of material.

In a recent paper (ref. 31), it was proposed that horizontal transport by such mechanisms as electrostatic charging has played a large role in the formation of the flat mare basins. It is obvious that if highland material had drifted into the basins to any extent, the differences between the mare and the surrounding highlands would not be perceived. In fact, very marked differences have been found and are demonstrated. There are outstanding examples such as the crater Tsiolkovsky. The ratio of aluminum in the rim area to that of the basin is about 2:1. Further, real differences can be discerned in such relatively homogeneous sites as the Serenitatis-Tranquillitatis zones and in the Tranquillitatis basin itself. There is additional substantiation in the recent paper of Kocharov and Viktorov (ref. 32) on the results obtained by the Lunokhod 2 in the crater Le Monnier. From the analysis of returned lunar samples, it has been found that the soils in the highland regions are generally like the highland rocks; and similarly in maria regions the soils are generally like the maria rocks. Thus it seems highly unlikely that these chemical differences arise because one type of rock is more easily broken up than another or more easily transported. It

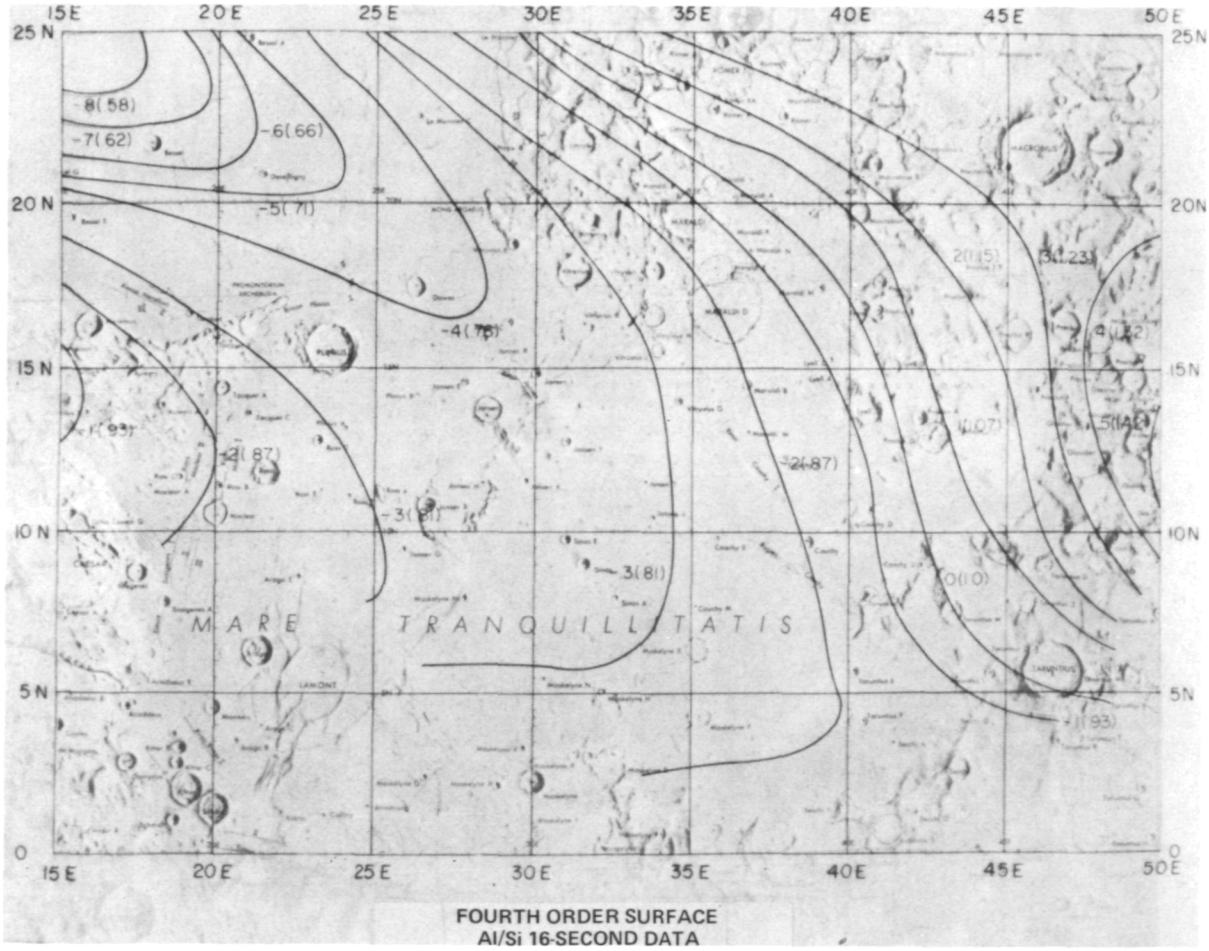

Figure 15.—*Fourth order trend surface map for Al/S intensity ratios using 16-second data (ref. 17).*

is questionable, therefore, whether small-scale, continuous, horizontal transport has played a large role in the formation of the flat maria basin.

Finally, short-time (8- and 16-second) X-ray fluorescence data were analyzed to determine their capability for mapping relatively small lunar features. Fluctuation in the solar spectral shape and variation of the look angle with spacecraft altitude make this type of analysis rather difficult, but some analysis can be performed and preliminary results have been obtained (ref. 17). Spatial mapping using trend surface analysis demonstrated that a usable signal could be abstracted from Al/Si intensity ratios compiled over short time periods. Residuals from the trend surface allowed isolation of similar areas. For details of the analytic method, see (ref. 17).

In this work a portion of Mare Serenitatis and Mare Tranquillitatis and their adjacent highlands observed during the Apollo 15 mission were chosen. On the basis of the analysis of variance interpretation using trend surface analysis of 16-second Al/Si ratio data, a fourth-order surface is the highest order which shows the proper level of significant improvement. Figure 15 (ref. 17) shows the derived model. Ratios are highest in the highlands to the northeast, and become progressively lower toward the mare. Low ratios are associated with the maria proper; the lowest values occur in Mare Serenitatis in the northwest portion of the mapped area. A high ratio is indicated by the Haemus Mountains in the western part of the map. The general model conforms well to the results discussed, in which the highlands have higher Al/Si intensity ratios than maria (figs. 11, 12, and 13).

Figure 16 (ref. 17) illustrates some selected anomalies based on the residuals from the fourth-order surface for the Al/Si ratio data.

Areas 10 and 11 and Area 3, representing Taurus-Littrow and Haemus highlands, respectively, show quite similar Al/Si ratios. Morris and Wilhelms (ref. 33) and Carr (ref. 34) mapped the Haemus highlands as Imbrian-age Fra Mauro formation, while the Taurus-Littrow highlands have been mapped as pre-Imbrian in age. As mentioned above, X-rays of the energy level measured during the Apollo missions have a penetration capability of 10μm; thus only surficial materials are mapped. Hence, it might be argued that Imbrian ejecta is being mapped in the Taurus-Littrow highlands, although it may form only a thin blanket. The crater Proclus covered in Area 21 displays considerably different Al/Si and Mg/Si ratios as compared with Area 20 ejecta material (refs. 35 and 36) derived from Proclus. These disparate results for materials of the same provenance may indicate stratigraphic variations within Proclus and the highlands.

Area 5, containing the crater Plinius, shows up as a distant positive anomaly from the maria materials as exemplified by Areas 4 and 6. The crater occupies an area interpreted as an impact crater (ref. 33) in an area of relatively thin mare materials at the transition between Mare Tranquillitatis and Mare Serenitatis. Crater excavation due to impact has most likely excavated and exposed highland material from the subsurface. Topographic data indicate that the crater was excavated to approximately 1200 meters below the mare floor. This sets a maximum limit for the mare thickness, which De Hon (ref. 37) estimates as 500 to 600 meters in this area.

Two additional positive mare anomalies which may be of significance are Areas 7 and 2. Area 7 corresponds to a wrinkle ridge and high albedo mare material as mapped by Carr (ref. 34). Examination of Apollo 15 metric photography indicates some features which might be interpreted as volcanic terrain or extrusive features. Both Young et al. (ref. 38) and Hodges (ref. 39) report possible extrusive igneous features in the same general vicinity. Low-albedo Mare Serenitatis materials are typified by ratios such as those in the negative residual of Area 1. This suggests that at least two types of substantially different mare basalts are present within Mare Serenitatis. Lowman (ref. 40)

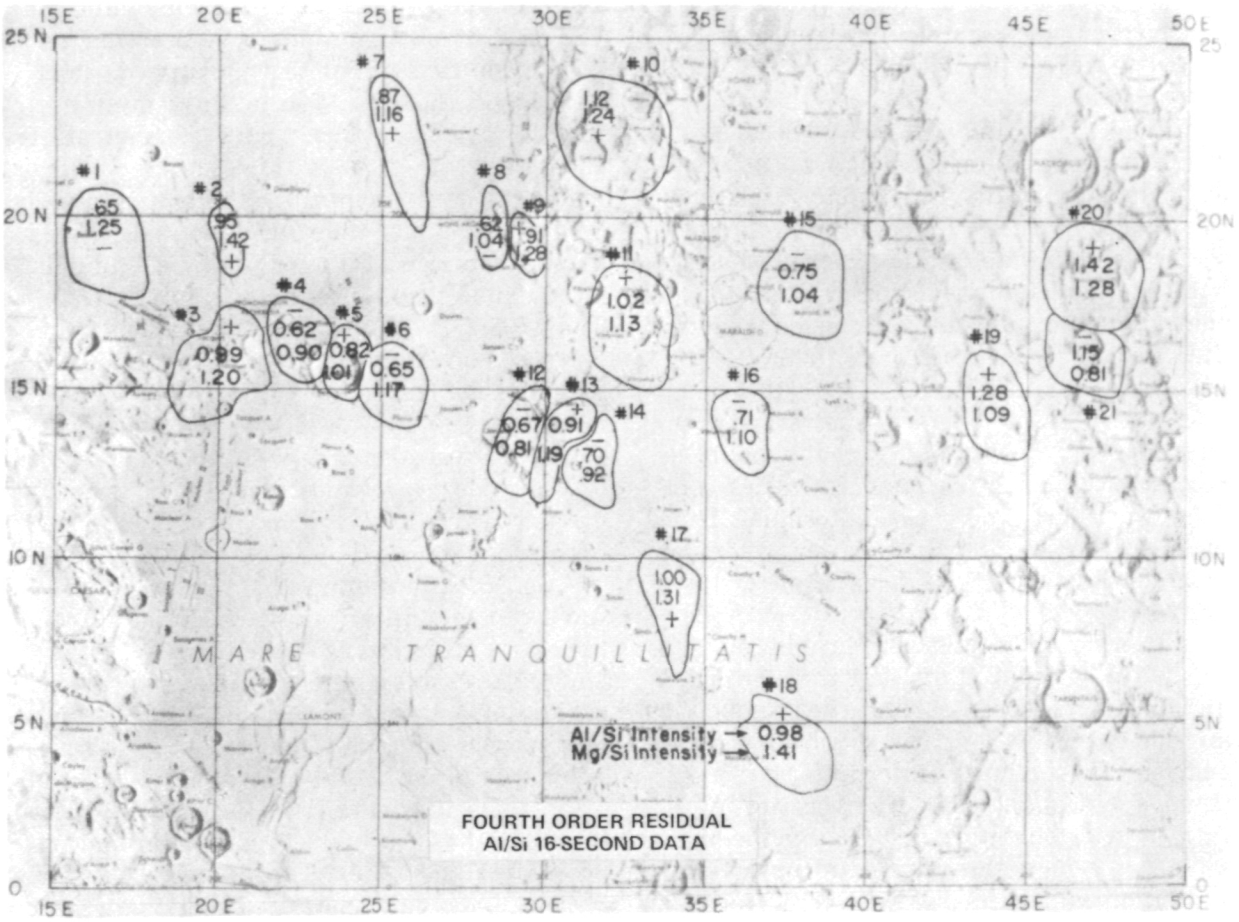

Figure 16.—*Residuals from the fourth order trend surface for Al/Si intensity ratios. Departures or deviations are based on normalized data. A plus sign denotes a positive residual; a negative sign indicates a negative residual. Calculated intensity ratios are given in original units for ease of interpretation (ref. 17).*

suggests that these wrinkle ridge areas may contain the final differentiation products of a large basaltic body and should contain higher alumina concentrations. Area 2, associated with a rectilinear junction of four mare ridges forming a parallelogram, also displays a similar positive anomaly.

Positive residuals associated with Areas 17 and 18 appear to be associated with zones of the highest albedo mare materials within Mare Tranquillitatis as mapped by Wilhelms (ref. 36). The positive residual associated with Area 13 is perplexing, for it is not associated with the Jansen craters as might be expected, but is located to their east. The only explanation for this anomaly at this time may be the concentration of ray materials as mapped by Morris and Wilhelms (ref. 33).

Conclusions

It is hoped that this summary and interpretation of results obtained from the Apollo X-ray and gamma-ray spectrometer experiment data presented here, will be helpful to investigators in the field of planetology. As can be seen from the results reported, the work is not yet completed, but much information was obtained. There is still much to be completed in the future.

Acknowledgment

The results reported in this work represent the efforts of persons too numerous to mention here. Appreciation is expressed to all these individuals for their help in the development, implementation, analysis, and interpretation of project results.

References

1. ARNOLD, J. R., L. E. PETERSON, A. E. METZGER, AND J. I. TROMBKA, *Preliminary Science Report*, NASA SP–289, 1972.
2. HARRINGTON, T. M., J. H. MARSHALL, J. R. ARNOLD, L. E. PETERSON, J. I. TROMBKA, AND A. E. METZGER, The Apollo Gamma-Ray Spectrometer. *Nuc. Instruments and Methods*, in press, 1974.
3. REEDY, R. C., J. R. ARNOLD, AND J. I. TROMBKA, Expected Gamma-Ray Emission Spectra From the Lunar Surface as a Function of Chemical Composition. *J. Geophys. Res.*, Vol. 78, 1973, pp. 5847–5866.
4. METZGER, A. E., J. I. TROMBKA, L. E. PETERSON, R. C. REEDY, AND J. R. ARNOLD, A First Look at the Lunar Orbital Gamma-Ray Data. *Proc. Third Lunar Science Conference, Geochimica et Cosmochimica Acta*, Supplement 3, Vol. 3, 1972, frontispiece.
5. METZGER, A. E., Lunar Surface Radioactivity: Preliminary Results of the Apollo 15 and Apollo 16 Gamma-Ray Spectrometer Experiments, *Science*, Vol. 179, 1973, pp. 800–803.
6. METZGER, A. E., J. I. TROMBKA, L. E. PETERSON, R. C. REEDY, AND J. R. ARNOLD, Element Concentration From Lunar Orbital Gamma-Ray Measurements. *Proc. Fifth Lunar Science Conference, Geochimica et Cosmochimica Acta*, in press, 1974.
7. REEDY, R. C., AND J. R. ARNOLD, Interaction of Solar and Galactic Cosmic Ray Particles With the Moon. *J. Geophys. Res.*, Vol. 77, 1972, p. 537.
8. LINGENFELTER, R. E., E. H. CANFIELD, AND V. E. HAMPEL, The Lunar Flux Revisited. *Earth Planet. Sci. Letters*, Vol. 16, 1972, p. 355.
9. FINKEL, R. C., M. IMAMURA, M. HONDA, K. NISHIIZUM', C. P. KOHL, S. M. KOCIMSKI, AND J. R. ARNOLD, Cosmic Ray Produced Mn and Be Radionuclides in the Lunar Regolith. *Proc. Fifth Lunar Science Conference, Geochimica et Cosmochimica Acta*, in press, 1974.
10. WOOLUM, D. S., AND D. S. BURNETT, In-Situ Measurement of the Rate of ^{235}U Fission Induced by Lunar Neutrons. *Earth Planet. Sci. Letters*, Vol. 21, 1974, p. 153.
11. TURKEVICH, A. L., E. J. FRANZGROTE, AND J. H. PATTERSON, Chemical Composition of the Lunar Surface in Mare Tranquillitatis. *Science*, Vol. 165, 1969, p. 277.
12. WAKITA, H., R. A. SCHMITT, AND P. REY, Elemental Abundances of Major, Minor and Trace Elements in Apollo 11 Lunar Rocks. *Apollo 11 First Lunar Science Conference, Geochimica et Cosmochimica Acta*, Supplement 1, Vol. 2, 1970, p. 1685.
13. SCHONFELD, E., AND C. MEYER, The Abundances of Components of the Lunar Soils by a Least Squares Mixing Model and the Formation Age of KREEP. *Proc. Third Lunar Science Conference, Geochimica et Cosmochimica Acta*, Supplement 3, Vol. 2, 1972, pp. 1397–1420.
14. ADLER, I., J. I. TROMBKA, J. GERARD, R. SCHMADEBECK, ET AL., X-Ray Fluorescence Experiment. *Apollo 15 Preliminary Science Report*, NASA SP–289, 1972.
15. ADLER, I., J. I. TROMBKA, R. SCHMADEBECK, P. LOWMAN, H. BLODGET, L. YIN, E. ELLER, M. PODWYSOCKI, J. R. WEIDNER, A. L. BICKEL, R. K. L. LUM, J. GERARD, P. GORENSTEIN, P. BJORKHOLM, AND B. HARRIS, Results of the Apollo 15 and 16 X-Ray Experiment. *Proc. Fourth Lunar Science Conference, Geochimica et Cosmochimica Acta*, Supplement 4, Vol. 3, 1973, pp. 2783–2791.
16. ADLER, I., M. PODWYSOCKI, C. ANDRE, J. I. TROMBKA, AND R. SCHMADEBECK, The Role of Horizontal Transport—As Evaluated From the Apollo 15 and 16 Orbital Experiments. *Proc. Fifth Lunar Science Conference, Geochimica et Cosmochimica Acta*, in press, 1974.
17. PODWYSOCKI, M. H., J. R. WEIDNER, C. G. ANDRE, A. L. BECKEL, R. S. LUM, I. ADLER, AND J. I. TROMBKA, An Analysis of the Apollo 15 X-Ray Fluorescence Experiment for Detailed Lunar Morphological and Geochemical Parameters. *Proc. Fifth Lunar Science Conference, Geochimica et Cosmochimica Acta*, in press, 1974.
18. TROMBKA, J. I., J. R. ARNOLD, R. C. REEDY, L. E. PETERSON, AND A. E. METZGER, Some Correlations Between Measurements by the Apollo Gamma-Ray Spectrometer and Other Lunar Observations. *Proc. Fourth Lunar Science Conference, Geochimica et Cosmochimica Acta*, Supplement 4, Vol. 3, 1973, pp. 2847–2853.
19. *Proc. Fourth Lunar Science Conference, Geochimica et Cosmochimica Acta*, Supplement 4, Vol. 1, 1973, frontispiece, plate II.
20. LSPET (Lunar Sample Preliminary Examination Team), *Science*, Vol. 173, 1971, p. 681.
21. SJOGREN, W. L., AND W. R. WOLLENHAUPT, Lunar Shape Via the Apollo Laser Altimeter. *Science*, Vol. 179, 1973, pp. 275–278.
22. COLEMAN, P. F., B. R. LICHTENSTEIN, C. T.

RUSSEL, G. SCHUBERT, AND L. R. SHARP, The Particles and Fields Subsatellite Magnetometer Experiment. *Apollo 16 Preliminary Science Report*, NASA SP–315, 1973.

23. ELDRIDGE, J. S., G. D. O'KELLEY, AND K. J. NORTHCUTT, Radionuclide Concentrations in Apollo 16 Samples. *Proc. Fourth Lunar Science Conference, Geochimica et Cosmochimica Acta*, Supplement 4, Vol. 2, 1973, p. 2115.
24. ELDRIDGE, J. S., G. D. O'KELLEY, AND K. J. NORTHCUTT, Abundances of Primordial and Cosmogenic Nuclides in Apollo 14 Rocks and Fines. *Proc. Third Lunar Science Conference, Geochimica et Cosmochimica Acta*, Supplement 3, Vol. 2, 1972, p. 1651.
25. O'KELLEY, G. D., J. S. ELDRIDGE, E. SCHONFELD, AND P. R. BELL, Abundances of the Primordial Radionuclides K, Th, and U in Apollo 12 Lunar Samples by Non-Destructive Gamma-Ray Spectrometry; Implications for Origin of Lunar Soils. *Proc. Second Lunar Science Conference, Geochimica et Cosmochimica Acta*, Supplement 2, Vol. 2, 1971, p. 1159.
26. ADLER, I., J. GERARD, J. I. TROMBKA, R. SCHMADEBECK, ET AL., The Apollo 15 X-Ray Fluorescence Experiment. *Proc. Third Lunar Science Conference, Geochimica et Cosmochimica Acta*, Vol. 3, David R. Criswell, ed., 1972, pp. 2157–2178.
27. ADLER, I., J. I. TROMBKA, J. GERARD, P. LOWMAN, R. SCHMADEBECK, H. BLODGETT, E. ELLER, L. YIN, R. LAMOTHE, P. GORENSTEIN, AND P. BJORKHOLM, Apollo 15 Geochemical X-Ray Fluorescence Experiment: Preliminary Report. *Science*, Vol. 175, 1972, pp. 436–440.
28. ADLER, I., J. I. TROMBKA, J. GERALD, P. LOWMAN, R. SCHMADEBECK, H. BLODGETT, E. ELLER, L. YIN, R. LAMOTHE, G. OSSWALD, P. GORENSTEIN, P. BJORKHOLM, H. GURSKY, AND B. HARRIS, Apollo 16 Geochemical X-Ray Fluorescence Experiment: Preliminary Report. *Science*, Vol. 177, 1972, pp. 256–259.
29. WHITAKER, E. A., *The Nature of the Lunar Surface, The Surface of the Moon.* Hess, Menzel, and O'Keefe, eds., The Johns Hopkins Press, 1965, p. 79.
30. PATTERSON, JAMES H., ANTHONY L. TURKEVITCH, E. J. FRANZGROTE, T. E. ECONOMOU, AND E. P. SOWINSKI, *Science*, Vol. 168, 1972, p. 825.
31. GOLD, T., *The Moon.* Vol. 7, Nos. 3 and 4, 1973.
32. KOCHAROV, G. E., AND S. V. VIKTOROV, Doklady, Akad. Nauk USSR, in press, 1974.
33. MORRIS, E. C., AND D. E. WILHELMS, Geologic Map of the Julius Caesar Quadrangle of the Moon. U.S. Geol. Survey, Map I–510, 1967.
34. CARR, M. H., Geologic Map of the Mare Serenitatis Region of the Moon, U.S. Geological Survey, Map I–489, 1966.
35. SCOTT, P. H., AND H. A. POHN, Geologic Map of the Macrobius Quadrangle of the Moon. U.S. Geol. Survey, Map I–799, 1972.
36. WILHELMS, D. E., Geologic Map of the Taruntius Quadrangle of the Moon. U.S. Geol. Survey, Map I–722, 1972.
37. DE HON, R. A., Thickness of Mare Material in the Tranquillitatis and Nectaris Basins. *Proc. Fifth Lunar Science Conference, Geochimica et Cosmochimica Acta*, in press, 1974.
38. YOUNG, R. A., W. J. BRENNAN, R. W. WOLFE, AND D. J. NICHOLS, Volcanism in the Lunar Maria. *Apollo 17 Preliminary Science Report*, NASA SP–330, 1973, pp. 31–1 and 31–11.
39. HODGES, C. A., Mare Ridges and Lava Lakes. *Apollo 17 Preliminary Science Report*, NASA SP–330, 1973, pp. 31–12 to 31–21.
40. LOWMAN, P., The Geologic Evolution of the Moon. *J. Geology*, Vol. 80, No. 2, 1972, pp. 125–166.